

Search for Stellar Flybys in the Sco-Cen OB Association with the Gaia DR2

YILUN MA (马逸伦) ¹, ROBERT J. DE ROSA ² AND PAUL KALAS ^{1, 3, 4}

¹*Department of Astronomy, University of California, Berkeley, CA 94720, USA*

²*European Southern Observatory, Alonso de Córdova 3107, Vitacura, Santiago, Chile*

³*SETI Institute, Carl Sagan Center, 189 Bernardo Ave., Mountain View CA 94043, USA*

⁴*Institute of Astrophysics, FORTH, GR-71110 Heraklion, Greece*

(Received June 21, 2021; Revised January 18, 2022; Accepted January 31, 2022)

Submitted to AJ

ABSTRACT

High-contrast imaging studies of debris disks have revealed a significant diversity in their morphologies, including large-scale asymmetries. Theories involving stellar flybys, an external source of gravitational disturbance, have offered a plausible explanation for the origin of these morphological variations. Our study is an experiment to gain empirical evidence that has been lacking from such theories. We explore this paradigm by using astrometric and radial velocity measurements from the *Gaia* DR2 and ground-based observations to trace the trajectories of 625 stars in the Sco-Cen OB Association from 5 Myr in the past to 2 Myr in the future. We identified 119 stars that had at least one past flyby event occurring within one Hill radius, and 23 of these experienced flybys within 0.5 Hill radius. We found no evidence of a significant correlation between the presence of flyby events and infrared excess detections, although the sample is not uniformly sensitive to infrared excess emission. Ten stars that had past flyby events host resolved circumstellar disks that appear relatively symmetric in the existing data except for the circumbinary disk surrounding HD 106906. We determined the trajectory and relative velocity of each of these flyby events, and compared these to the geometry of the spatially-resolved disks. Future work is needed to measure the kinematics of lower mass stars and to improve sensitivity to circumstellar disks for the entire sample.

Keywords: Celestial mechanics (211), Close encounters (255), Debris disks (363), Circumstellar disks (235)

1. INTRODUCTION

Our planetary system is mostly flat and symmetric with the terrestrial and giant planets orbiting nearly in the same plane with low eccentricities. However, highly eccentric orbits and misalignments in extrasolar planetary systems (e.g., high mutual inclinations, disk-planet misalignments, disk asymmetries, etc.) are not unusual (e.g., Kalas & Jewitt 1995; Tamuz et al. 2008; Triaud et al. 2010; Kennedy et al. 2012; De Rosa et al. 2020). One mechanism to explain high eccentricities is planet-planet scattering, a form of internal dynamical excitation (e.g., Rasio & Ford 1996; Raymond et al. 2010). How the scattering starts out in the first place can be attributed to planet migration in gaseous circumstellar disks, thus disrupting the primordial orbital configuration of the system (Kley & Nelson 2012).

However, external stellar and sub-stellar perturbers can also reshape the architectures of planetary systems. Such perturbers can be bound to the system in cases of stellar multiplicity or distant planet-mass objects, or unbound in the case

of stellar or sub-stellar flybys. An example of the bound stellar case is the RW Aur system. Cabrit et al. (2006) and Rodriguez et al. (2018) suggested that periastron passages between RW Aur A and B could explain the asymmetric features of the RW Aur B disk and the trailing material from the RW Aur A disk. An example of the bound sub-stellar case is the 11 M_J mass exoplanet HD 106906 b which orbits exterior to the distorted circumbinary debris disk (Kalas et al. 2015) and which could explain the disk's asymmetric morphology (Nesvold et al. 2017; Rodet et al. 2017; Nguyen et al. 2021). If the planet originally formed in the disk and evolved outward due to interior instabilities, unbound stellar flybys may have raised its periastron distance away from the central planetary region (Rodet et al. 2017; De Rosa & Kalas 2019). Thus the HD 106906 system has evidence for both internal and external perturbations at play.

Stellar flyby events have occurred during our own solar system's history as well. The existence of dynamically new, long-period comets entering the inner solar system at random

inclinations is consistent with a scenario where primitive icy bodies were ejected to large aphelia by the giant planets, had their perihelia raised and inclinations randomized by perturbations from passing stars, and approach the Sun again at later epochs when their perihelia are decreased by other passing stars (Oort 1950; Hills 1981; Duncan et al. 1987). For example, Mamajek et al. (2015) found that the low-mass binary WISE J072003.20084651.2—also known as “Scholz’s star”—had a flyby with our Sun at 0.25 pc roughly 70,000 years ago. This is the closest flyby event with our solar system discovered to date. Using *Gaia* DR2 data, Bailer-Jones et al. (2018) calculate that Gl 710 (HIP 89825) will come within 0.09 pc of the Sun ~ 1.2 Myr in the future and estimate that roughly 20 stars per Myr pass within 1 pc of the Sun.

Alternately, long-period comets may have been captured at early times (e.g., age < 10 Myr) when the Sun still resided in its birth cluster and small bodies were ejected from their original formation sites around other stars due to flybys (Levison et al. 2010). The high mutual inclination and eccentricity of certain Kuiper Belt objects may be signatures of past stellar flybys of the proto-Sun with other members of the Sun’s natal cluster after the gas giants had formed (Ida et al. 2000; Kenyon & Bromley 2004; Kobayashi et al. 2005; Pfalzner et al. 2018).

Theoretical work has generally explored how the architectures of exoplanetary systems could be modified in a young cluster environment by flybys. At the earliest epochs the structure of protoplanetary disks may be altered, such as by having disk outer radii truncated (Larwood 1997; Rosotti et al. 2014; Winter et al. 2018; Cuello et al. 2019). Close stellar encounters can also create spiral structure, asymmetric rings, and vertically disturbed populations of particles that may account for observed debris disk asymmetries (Larwood & Kalas 2001; Reche et al. 2009; Lestrade et al. 2011; Cuello et al. 2020). Encounters between a planetary system and a flyby star could excite the eccentricity of the outer planets and transfer the excitation of eccentricity inward on a longer timescale (Zakamska & Tremaine 2004). Flybys could also completely eject outer planets from the system and leave the surviving planetary system unstable (Hills 1984; Malmberg et al. 2011; Parker & Quanz 2012).

In this paper, we extend the De Rosa & Kalas (2019) study of the HD 106906 system to the entire Sco-Cen OB association, identifying the possible stellar flybys among its members using a combination of astrometry and radial velocities from *Gaia* DR2 (Gaia Collaboration et al. 2018) and from various other literature sources. In Section 2, we describe the characteristic of the samples used in this study, such as mass estimation and sample completeness. In Section 3, we present the procedure used to identify stellar flybys in the samples. The results that comes out of those methods are pre-

sented in Sections 4.1 and 4.2. In Section 4.3, we discuss the correlation between the presence of infrared excess (IR) and stellar close approaches. Section 4.4 then focuses on close approaches involving stars hosting resolved debris disk and presents the flyby geometry of those with determined disk orientations. Section 5 discusses potential encounters identified in the Upper Scorpius subgroup via simulating precise RV measurements. Lastly, Section 6 summarizes the findings and discusses potential future development.

2. SAMPLE PROPERTIES

2.1. Sample Selection

This study used the three-dimensional positions and motions of the known members of the nearby (116 – 144 pc, de Zeeuw et al. 1999) Scorpius-Centaurus OB2 association to identify close stellar approaches. The positions and motions were derived from precise *Gaia* Data Release 2 (DR2) astrometry (Gaia Collaboration et al. 2018) and a combination of *Gaia* and ground-based radial velocity (RV) measurements. The study focused on two samples of stars from this association: the first based on a census of stars in the region from the *Hipparcos* satellite (ESA 1997), and the second based on a revised census of the Upper Scorpius (US) subgroup using data from *Gaia* DR2.

The first sample, which we call the “Sco-Cen” sample, was a subset of a catalog of Sco-Cen members constructed based upon Wright & Mamajek (2018) and Song et al. (2012), which contains 539 stars from all three subgroups of the association — Upper Scorpius (USCO), Upper Centaurus-Lupus (UCL), and Lower Centaurus-Crux (LCC). The subset we used in this study contains 462 catalog stars that have a radial velocity measurement from either *Gaia* or ground-based instruments. When a target had a RV measurement from both *Gaia* and other facilities, we opted to use the measurement with the lowest uncertainty. A full listing of the Sco-Cen sample is given in Table 2.

The second group, which we call the “USCO” sample, is derived from 1682 stars in the *Gaia* DR2 catalog that are identified as USCO members in Table 4 of Luhman & Esplin (2020). We excluded 120 stars missing parallax measurements and 2 stars with negative parallax measurement and obtained a reduced sample of 1560 stars. This sample included 56 stars which are in the Sco-Cen sample described above. Among the stars in the USCO sample, 219 have RV from either the *Gaia* catalog or ground-based measurements, and we adopt the same procedure for targets with RV measurements from both *Gaia* and other facilities as with the other sample. A full listing of the USCO sample is given in Table 3. In total the two samples consist of 625 unique targets.

2.2. Mass Estimation

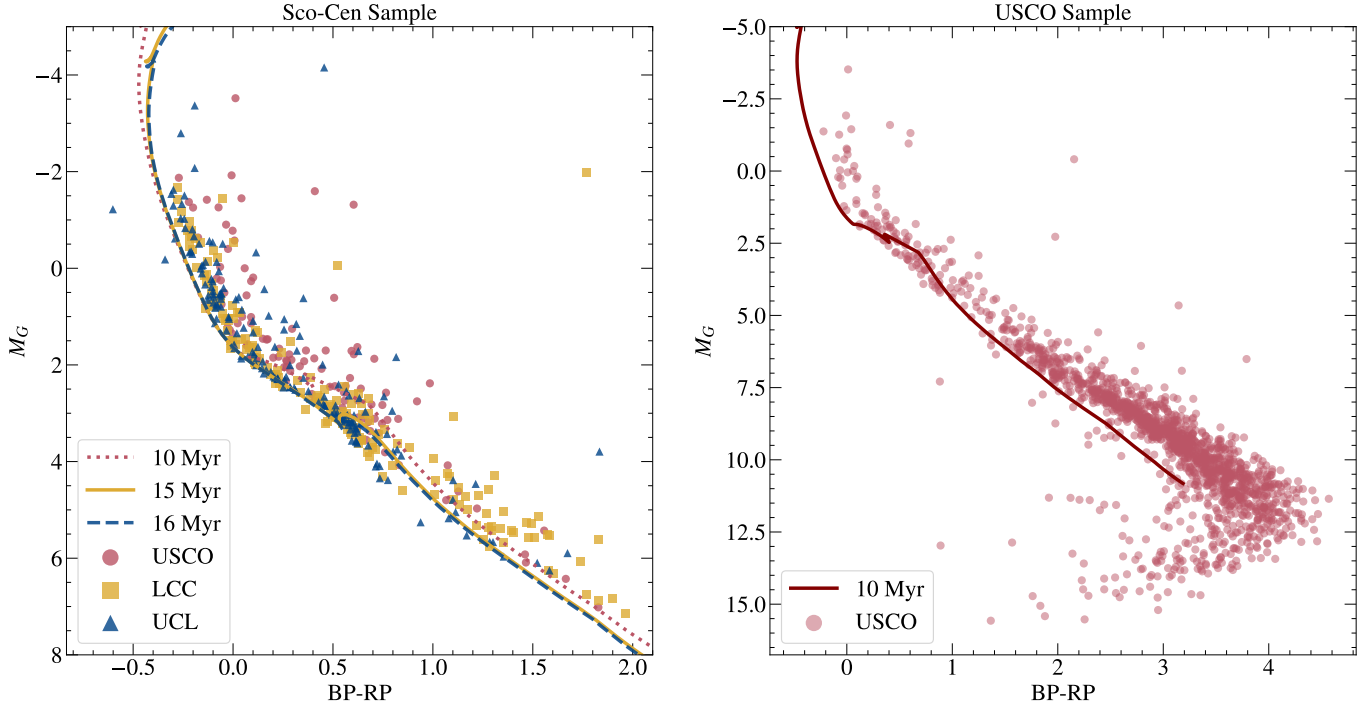


Figure 1. Color-magnitude diagram of the two samples created using optical photometry from *Gaia* DR2. Some stars that are not on the main sequence are not plotted. Isochrones from MIST at the ages of the three subgroups are also plotted for comparison. No extinction correction is applied to either the sample or the isochrones.

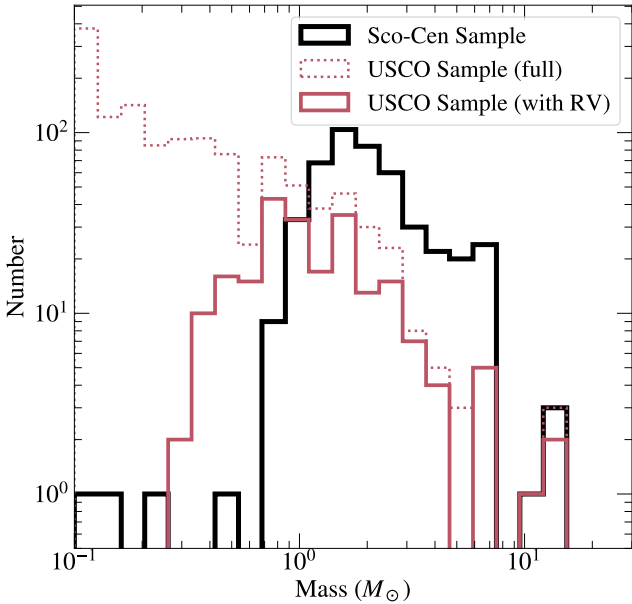


Figure 2. The mass distributions of the samples are plotted. The full samples are plotted with solid lines; the mass distributions of USCO stars with RV is plotted with the dotted line. The bin are drawn in the logarithmic space.

To assess the relative significance of stellar flybys identified in this study, we required an estimate of the mass of each star within both samples. We generated color-magnitude di-

agrams (CMDs) of the two samples using optical photometry from *Gaia*. Plotted in Fig. 1, these clearly demonstrate that the Sco-Cen sample is restricted to more luminous stars ($M_G \lesssim 7$) due to the sample being primarily derived from *Hipparcos* astrometry, whereas the USCO sample includes stars that are as faint as $M_G \sim 15$. To assess the completeness of the two samples, we derived the stellar masses of the two samples based on the stars’ spectral types. We first interpolated a relation between spectral type and effective temperature based on Table 5 of Pecaut & Mamajek (2013). We then modelled the isochrones for the three subgroups with the MESA Isochrones and Stellar Tracks (MIST) (Paxton et al. 2011, 2013; Dotter 2016; Choi et al. 2016), assuming the ages of USCO, UCL, and LCC to be 10 Myr, 16 Myr, and 15 Myr, respectively (Pecaut & Mamajek 2016), and the metallicities of the subgroups to be solar for simplicity (Viana Almeida et al. 2009). We obtained a relation between effective temperature and stellar mass, and thus between spectral type to stellar mass for each subgroup individually. For stars whose derived effective temperature is not covered by the isochrones, we used a luminosity-mass relation from the MIST isochrones and estimated their stellar masses using their G-band magnitudes in *Gaia* DR2. We did not apply any extinction correction to the optical magnitudes as we do not require precise masses, although the extinction towards many of the sources in both samples is expected to be small (e.g. Pecaut & Mamajek 2016).

We generated the mass distribution of the two samples using the derived masses, which is shown in Fig. 2. For stars whose derived effective temperatures are so low that they exceed the isochrones’ coverage, we assumed the mass to be $0.1 M_{\odot}$, which causes a slight over-abundance of stars at the low-mass end of the mass distribution for the USCO sample. Based on the mass distributions, we found that the USCO sample is indeed bottom-heavy and matches the IMF quite well, while the Sco-Cen sample is deficient of lower-mass stars. The Sco-Cen sample is complete to $\sim 1M_{\odot}$, and the USCO sample indeed includes more low-mass stars and is complete down to $\sim 0.1M_{\odot}$. However, although the USCO sample has more stars with RV measurements at the low-mass end than the Sco-Cen sample does, the RV measurement is still incomplete for the star with $M \lesssim 0.3 M_{\odot}$.

Ideally, we would have a more complete sample for the LCC and UCL subgroups as well in order to trace the dynamics of the subgroups more comprehensively. However, since a thorough census of these two sub-groups had not yet been performed using *Gaia* DR2 astrometry, we decided not to mix the two samples and treat them separately to avoid bias against the two less-sampled subgroups.

3. METHODS

3.1. Flyby Identification

The astrometry and radial velocities are used to trace the stellar motion of the stars in both samples from 5 million years in the past to 2 million years in the future. We assumed that the stars are gravitationally unbound with each other and the time interval integrated over is short comparing to the galactic orbital periods of the stars so that the effect of the galactic potential can be neglected. Therefore, the trajectories of the stars can be approximated as linear. In their analysis of stellar flybys of HD 106906, De Rosa & Kalas (2019) showed that there is not a significant deviation in the result between the linear approximation and an N-body simulation. We assumed that this is true for all of the stars within both samples. Based on the linear approximation, we computed the time of closest approach t_{ca} between any pair of stars in the sample as

$$t_{ca} = -\frac{(\mathbf{r}_2 - \mathbf{r}_1) \cdot (\mathbf{v}_2 - \mathbf{v}_1)}{|\mathbf{v}_2 - \mathbf{v}_1|^2}, \quad (1)$$

where \mathbf{r}_1 , \mathbf{r}_2 and \mathbf{v}_1 , \mathbf{v}_2 represent the pairs of positions and velocities of the two stars. Subsequently, we are able to compute the distance of closest approach d_{ca} of each pair of stars as

$$d_{ca} = |(\mathbf{r}_2 - \mathbf{r}_1) + (\mathbf{v}_2 - \mathbf{v}_1)t_{ca}|. \quad (2)$$

Uncertainties of the *Gaia* astrometry and the radial velocity (RV) measurement are propagated with a Monte Carlo (MC) fashion. For each of the 10^6 trials, we drew the position, parallax, and proper motion of both stars based on a

multivariate normal distribution using the correlation coefficients in the *Gaia* DR2 catalog and drew the radial velocities from a separate Gaussian distribution. Using Equation 1 and Equation 2, t_{ca} and d_{ca} were computed for all 10^6 trials. We used the median values of t_{ca} and d_{ca} as the adopted values for these parameters, and the 16th- and 84th-percentiles were used as the lower and upper bounds, respectively.

We used the star’s Hill radius R_H under the galactic potential as a mass-weighted distance to classify the flybys. The Hill radius encodes the radial boundary of a volume where a star has a greater gravitational influence on an object than the galactic potential. The Hill radii were approximated using

$$R_H \approx a \left(\frac{m_{\star}}{3M_{enc}(a)} \right)^{\frac{1}{3}}, \quad (3)$$

where a is the distance from the galactic center to the star, m_{\star} is the derived stellar mass, and $M_{enc}(a)$ is the mass enclosed within the star’s galactic orbit assuming a flat rotation curve for our Galaxy. If $d_{ca} < 0.5R_H$ for either star, it is categorized as a “close encounter.” If $0.5R_H \leq d_{ca} \leq R_H$ (for either star), then the event is called an “encounter.” For more generic references to unbound interactions we use the term “flyby.” We do not use these terms to refer to the periastron passages of bound objects even if the orbits are highly eccentric and with large semi-major axes. Tables 3–5 have columns $d_{ca}/R_{H,T}$ and $d_{ca}/R_{H,F}$ where the former lists how the closest approach distance compares to the Hill radius of the target (T) and the latter with respect to the Hill radius of the flyby star (F).

3.2. Flyby Geometry

For each flyby event that involve a resolved debris disk, we also derived the geometry of the closest approaches. Assuming the disks are azimuthally symmetrical centered around their host stars, we used four reference points around the disk edge to carry out rotations that eventually leads to orienting the disks in galactocentric coordinates, the coordinate system we used for calculating the flyby timing and distances. These reference points are defined as

$$\mathbf{p}_1 = \begin{bmatrix} 0 \\ r/d \\ 0 \end{bmatrix}, \mathbf{p}_2 = \begin{bmatrix} 0 \\ -r/d \\ 0 \end{bmatrix}, \mathbf{p}_3 = \begin{bmatrix} 0 \\ 0 \\ r/d \end{bmatrix}, \mathbf{p}_4 = \begin{bmatrix} 0 \\ 0 \\ -r/d \end{bmatrix}, \quad (4)$$

where d is the distance to the host star and r is a nominal radius of the disk measured from the resolved images. The origin (0, 0, 0) is defined to be the position of the host star, and the three axes are along the RA, DEC, and line-of-sight directions, respectively. We carried out the first rotation based on the position angle (PA) of the disk via the rotation matrix

$$\mathbf{R}_{\theta} = \begin{bmatrix} \cos(\text{PA}) & \sin(\text{PA}) & 0 \\ -\sin(\text{PA}) & \cos(\text{PA}) & 0 \\ 0 & 0 & 1 \end{bmatrix}. \quad (5)$$

To rotate the reference points according to the inclination of the disk, we first defined the normal vector about which this second rotation was carried out as

$$\hat{\mathbf{n}} = \mathbf{R}_\theta \left(\frac{\mathbf{p}_2 - \mathbf{p}_1}{|\mathbf{p}_2 - \mathbf{p}_1|} \right). \quad (6)$$

Thus, we constructed our inclination-rotation matrix as

$$\mathbf{R}_i = \begin{bmatrix} (1-s) + n_1^2 s & n_1 n_2 s - n_2 c & n_2 n_3 s + n_2 c \\ n_1 n_2 s + n_3 c & (1-s) + n_2^2 s & n_2 n_3 s - n_1 c \\ n_1 n_3 s - n_2 c & n_2 n_3 s + n_1 c & (1-s) + n_3^2 s \end{bmatrix}, \quad (7)$$

where $s = 1 - \sin i$, $c = \cos i$ and n_1 , n_2 , and n_3 are the three components of $\hat{\mathbf{n}}$, respectively. After correcting the projection on the sky plane, we add the offset of the stars' positions in Cartesian ICRS coordinates to all four points to transform from the star frame to the ICRS coordinate frame. We then transformed these four points from ICRS to galactocentric coordinates using the procedures defined in `astropy.coordinates`. In the galactocentric coordinates, we define the normal vector of the debris disk as

$$\hat{\mathbf{N}} = \frac{(\mathbf{p}'_1 - \mathbf{p}'_2) \times (\mathbf{p}'_3 - \mathbf{p}'_4)}{|(\mathbf{p}'_1 - \mathbf{p}'_2) \times (\mathbf{p}'_3 - \mathbf{p}'_4)|}, \quad (8)$$

where the primed vectors are the galactocentric coordinates of the reference points. We then calculated the closest approach angle θ_{ca} , the angle between the disk plane and the flyby star's velocity vector (\mathbf{v}_{rel}) in the rest frame of the target star, as

$$\theta_{ca} = \arcsin \left(\frac{\hat{\mathbf{N}} \cdot \mathbf{v}_{rel}}{|\mathbf{v}_{rel}|} \right). \quad (9)$$

The uncertainties on all properties were propagated in a Monte Carlo fashion. The angle of closest approach defined previously is calculated for each of the 10^6 draws, where we drew disk position angles and inclinations from Gaussian distributions using the literature measurement and uncertainty. We validated our implementation of this algorithm by comparing to the results for HD 106906 presented in [De Rosa & Kalas \(2019\)](#).

4. RESULTS

4.1. Flyby Statistics

In the Sco-Cen sample, we identified seven past *close* encounters and seven future close encounters, each involving 13 stars, along with 37 past encounters and 28 future encounters involving 63 and 45 stars, respectively. There are 98 individual stars involved in all these events (including both encounters and close encounters). Similarly, we carried out the same calculation on 219 stars in the USCO sample where we identified 18 past close encounters involving 33 stars, 7 future close encounters involving 13 stars, 60 past encounters involving 81 stars, and 39 future encounters involving 64

stars. In total, 116 individual stars are involved in all these events. The time and distance of closest approach events of both samples are presented in Figures 4 and 5. As the time approaches the present, more encounters and close encounters are identified. We attribute this phenomenon to the increasing uncertainties of d_{ca} and t_{ca} as we trace further back to the past and into the future due to the non-zero uncertainties of the astrometry and radial velocities, an effect also seen in studies of stellar encounters with our own solar system (e.g., [Bailer-Jones et al. 2018](#)). The full list of flyby events is presented in Table 4.

The spatial distribution of flybys in both samples is presented in Fig. 3. We observe that stars involved in flybys are distributed evenly in the sky, except for a deficiency of events between $\ell = 314^\circ$ and $\ell = 334^\circ$. This gap in the spatial distribution of flybys is coincident with a lower density of stars seen on the western side of the UCL subgroup. The lower density within this region is also seen in the spatial distribution of fainter pre-main sequence candidate members identified from an analysis of *Gaia* DR2 data (e.g., [Damiani et al. 2019](#)). The lower occurrence of identified flybys within this region can simply be ascribed to a lower three-dimensional density of stars within this part of the association.

The algorithm we used to identify flybys would naturally include some wide binaries due to the fact that they share similar positions and velocities. According to the Washington Double Star Catalog (WDS; [Mason et al. 2020](#)), in the Sco-Cen sample, 22 out of the 98 Sco-Cen stars involved in flybys have binary companions; 16 out of the 116 USCO stars involved in flybys have binary companions as well; however, none of the identified flyby pairs is listed as physically associated. Nonetheless, HD 143844 and HD 143215, which are identified to have a flyby event, are identified as wide binaries in [Hartman & Lépine \(2020\)](#). Four other flyby events that we identified (HD 144587 / HD 144175, HD 146897 / HD 147083, HD 137499 / HD 137432, and HD 121835 / HD 121190) are also catalogued to be wide binary systems by [Jiménez-Esteban et al. \(2019\)](#). However, it is very difficult to determine whether a wide pair is gravitationally bound given the very low relative orbital velocities and the current radial velocity uncertainties for many of these stars. It is also worth noting that when tracing the trajectories, the radial velocity measurements of some stars that are in short-period binary systems may not be representative of the systematic velocity, which would cause an incorrect determination of the three-dimensional trajectories of these stars. Where possible we used systemic velocities for spectroscopic binaries derived from orbit fits presented in the literature (e.g., [Levato et al. 1987](#)).

4.2. Field Star Flybys

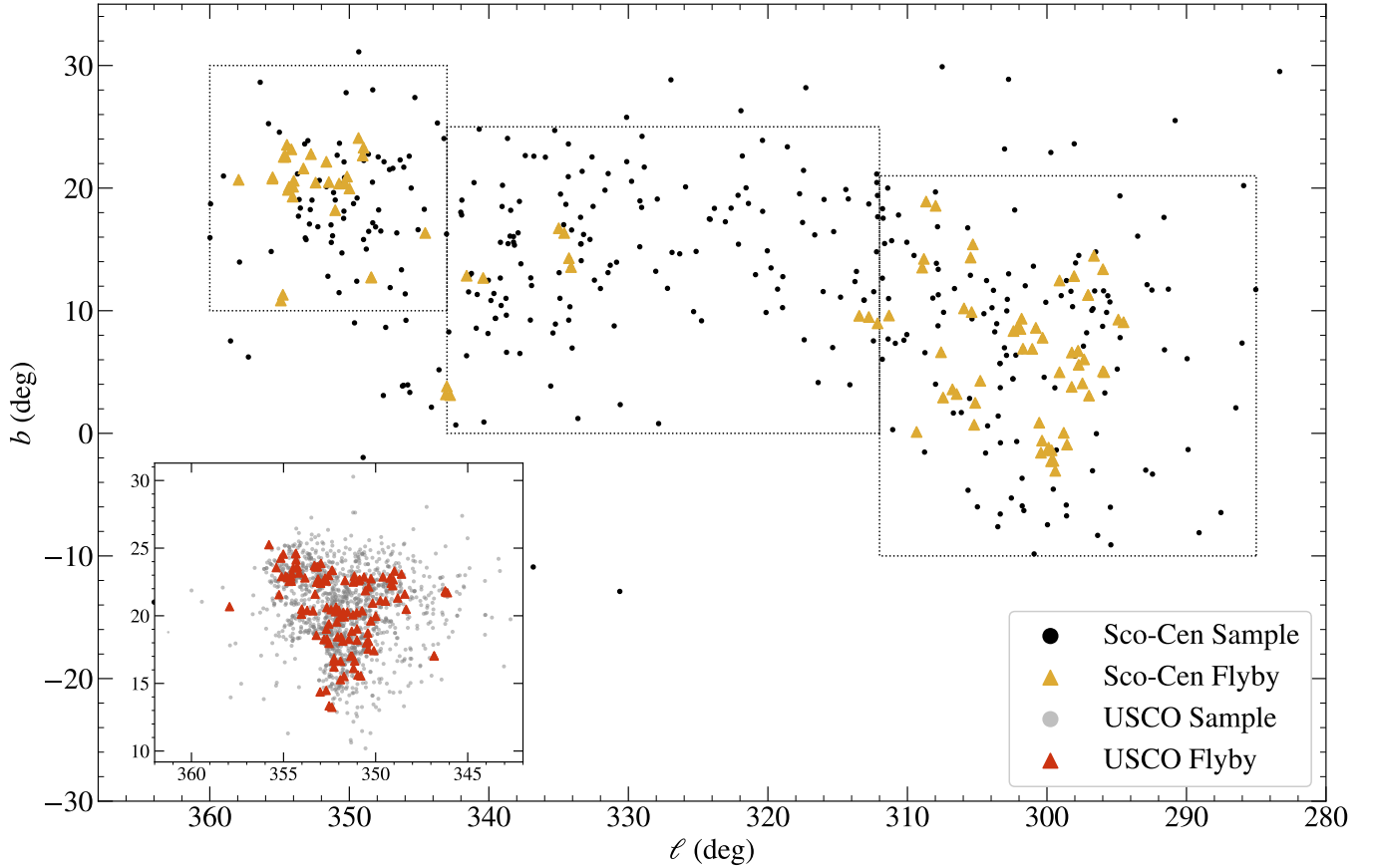


Figure 3. The spatial distribution of the two samples as well as the stars with identified flyby events is plotted in the Galactic coordinates. The dashed boxes mark the boundaries of USCO, UCL, and LCC identified by [de Zeeuw et al. \(1999\)](#). The USCO sample is plotted within the inset.

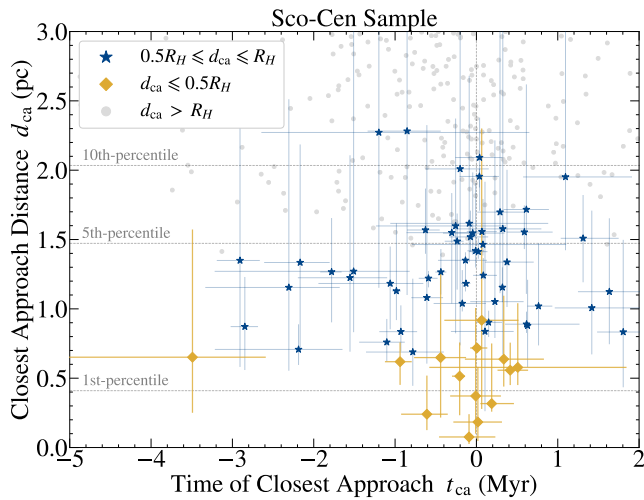


Figure 4. Closest approach times and distances for the encounters and close encounters identified in the Sco-Cen sample. Orange diamonds mark the close encounters ($d_{ca} \leq 0.5R_H$); blue stars mark encounters ($0.5R_H \leq d_{ca} \leq R_H$); gray dots mark the pairs whose close approach distance is in neither star’s Hill radius. The dotted horizontal lines mark the 1st-, 5th- and, 10th-percentiles of the distribution of the separation of stars within the sample. The median separation of stars in the Sco-Cen sample is 5.60 pc.

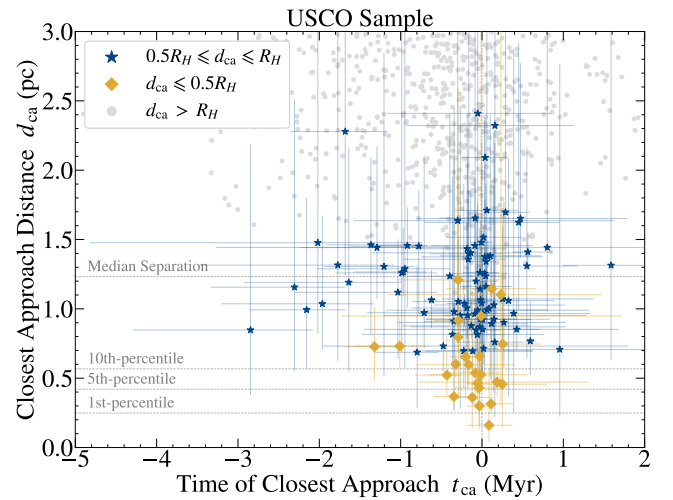


Figure 5. Closest approach times and distances for all the encounters and close encounters identified in the USCO sample. Legends are the same as that in Fig.4. The median separation of stars in this sample is 1.23 pc.

We also ran our closest approach algorithm on a dataset combining all stars in the *Gaia* DR2 that were not a part of either of the Sco-Cen samples that have RV measure-

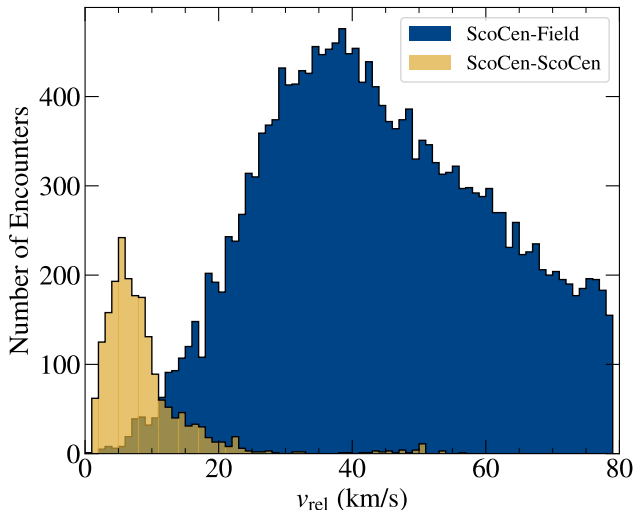


Figure 6. The comparison of relative velocity distributions between ScoCen-Field encounters (blue) and ScoCen-ScoCen encounters (orange) with $d_{ca} < 3$ pc.

ments from either *Gaia* or other ground-based observations reported in SIMBAD. Among this dataset, we flagged the stars that are identified by Damiani et al. (2019) as candidate Sco-Cen members based on their *Gaia* DR2 astrometry. Those that are not flagged are hereafter referred to as the field sample or field stars. This field sample consists of approximately 7.5 million stars, with greater completeness than the Sco-Cen sample to low-mass stars ($0.5\text{--}1 M_{\odot}$) owing to the magnitude and effective temperature range of stars with *Gaia* DR2 radial velocities.

We found that flybys involving field stars with $d_{ca} < 3$ pc are significantly more frequent than those only involving members of the Sco-Cen sample, in large part due to the difference in completeness between the two samples. However, the two types of flyby (ScoCen-Field vs. ScoCen-ScoCen) have different relative velocity distributions as shown in Fig. 6. The median relative velocity for encounters between Sco-Cen members and field stars is ~ 45 km/s, whereas that for encounters between two Sco-Cen members is ~ 7 km/s.

If we use the change in orbital speed as a measure for dynamical influence (e.g., Kalas et al. 2001), we see this difference in relative velocity causes a factor of ~ 6 difference between the two types of encounters. Furthermore, it can be observed in Fig. 7 that the events with $d \lesssim 1$ pc and $v_{rel} \lesssim 10$ km/s are dominated by encounters between members of the association. From this we infer that it is the encounters between members of the association that are more dynamically important than with field stars. Nevertheless, we report the details of encounters with field stars, and with candidates from Damiani et al. (2019), in Table 6.

4.3. Correlation with infrared excess

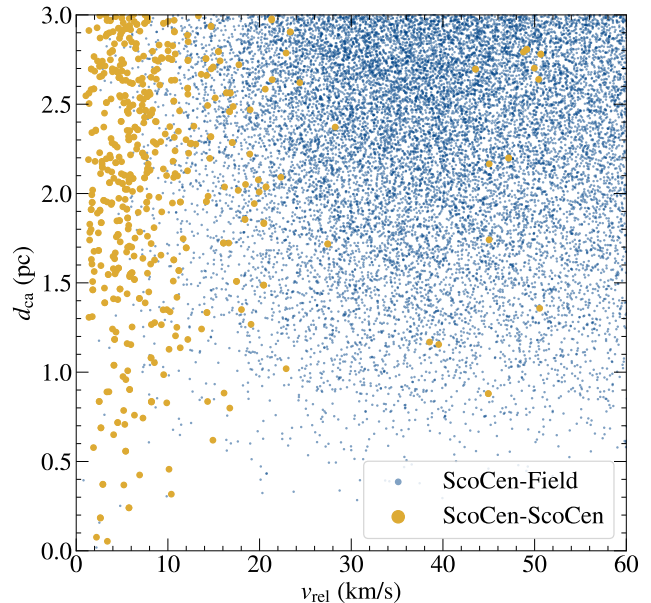


Figure 7. The closest approach distance is plotted against relative velocity for ScoCen-field encounters (blue) and ScoCen-ScoCen encounters (orange).

Various effects are possible when close stellar flybys interact with a star surrounded by a disk of planetesimals and/or planet-mass objects. The flyby can strip away outer material, truncating a circumstellar disk, but also increasing the volume density of surviving material and dynamically heating it (Pfalzner et al. 2005; Lestrade et al. 2011). This would increase the rate of dust-producing collisions, manifesting as an infrared excess until the entire system dynamically relaxes and dust grains are depleted by collisional destruction, sublimation, or removal by radiation forces. The 5 Myr-old HD 141569 debris disk may be undergoing this process at the current epoch due to the flyby of one or more M stars (Weinberger et al. 2000; Augereau & Papaloizou 2004; Ardila et al. 2005). To test for a possible correlation between flybys and IR excesses, we crosschecked both of our samples with the list of IR excess stars compiled in Cotten & Song (2016) and determined the fraction of the sample stars with excess. In the Sco-Cen sample, we identified 126 stars with IR excess with the dust temperature between 50K and 575K; 33 out of 67 events involve 24 IR-excess stars. In the USCO sample, there are 42 IR-excess stars with the dust temperature ranging from 75 K to 450 K; 21 out of 117 events involve 9 IR-excess stars.

As shown in Figure 8, the distributions of the close approach distance for stars with and without IR excess overlap for the Sco-Cen sample. However, since the Cotten & Song (2016) study does not have a uniform sensitivity for the IR excess detection for all the stars and the sample itself is less complete for the low mass stars, we would conservatively

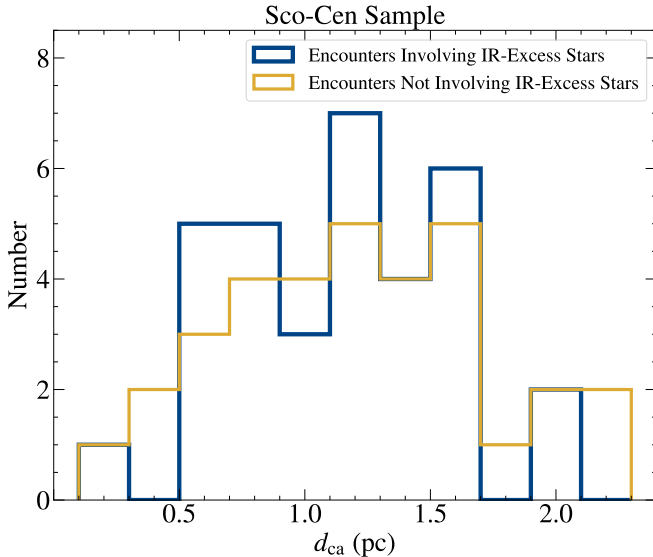


Figure 8. The comparison of the close approach distances of the events involving and not involving IR-excess stars for the Sco-Cen sample.

conclude that our data do not provide evidence for a correlation between the presence of IR excess and stellar flybys. For the same issue of sensitivity, only 42 out of 1560 stars in the USCO sample are included in Cotten & Song (2016). Most stars in the USCO sample were too faint to be catalogued and have only been recently identified with data from the *Gaia* satellite, which makes the sample bias more significant. Consequently, we did not include USCO sample in this analysis.

4.4. Flybys of stars with disks detected in scattered light or with ALMA

To search for morphological evidence of dynamical interactions between stellar flybys and circumstellar material (e.g., radial asymmetries, spiral structures, and vertical warps), we surveyed the literature for resolved detections of debris disks around the stars identified as having flyby events with other association members in the past. Table 1 and Fig. 9 present the flyby parameters, including the current 3D separations between stars (d_0), the relative velocities of each flyby (v_{rel}), and the relative angles between the disk midplanes and flyby trajectories (θ_{ca}).

Out of all the flyby stars from both samples, five have debris disks resolved in *scattered light* at visible and/or near-infrared wavelengths: HD 106906, HD 114082, HD 115600, HD 146897, and 2MASS J16042165-2130284 (RXJ1604.3-2130). At thermal wavelengths, the Atacama Large Millimeter/Submillimeter Array (ALMA) has been used to resolve the disks surrounding 2MASS J16064794-1841437 and HD 145718 (Ansdell et al. 2020). In the USCO sample, 2MASS J16035767-2031055 hosts a circumstellar disk (Luhman &

Mamajek 2012) also resolved with ALMA at 0.88 mm continuum and the CO $J = 3 - 2$ line at 345.8 GHz (Barenfeld et al. 2016). Circumstellar dust disks were weakly detected (SNR \sim 3–4) but unresolved at 1.24 mm by Lieman-Sifry et al. (2016) using ALMA with \sim 1'' resolution around HD 113556 and HD 142315. We include these two disks in our discussion to anticipate the availability of higher resolution continuum maps in the near future. We discuss the details of all 10 cases below.

4.4.1. HD 106906

We confirm the De Rosa & Kalas (2019) result that HD 106906 (F5V) has experienced two flyby events: one close encounter with HD 106444 (F5V) at $d_{ca} = 0.65^{+0.92}_{-0.40}$ pc and $t_{ca} = -3.49^{+0.90}_{-1.75}$ Myr and an encounter with HIP 59721 (G9V) at $d_{ca} = 0.71^{+0.18}_{-0.11}$ pc and $t_{ca} = -2.19^{+0.54}_{-1.03}$ Myr. The two candidate perturbers likely form a wide binary system (Mason et al. 2001). The two events are only separated by \sim 1.5 Myr and are nearly co-planar, the closest approach angles are $5.90^{+1.77}_{-1.67}$ deg and $4.64^{+1.00}_{-1.16}$ deg, respectively.

An asymmetric inner disk is observed in *H*-band scattered light (Kalas et al. 2015; Lagrange et al. 2016). Moreover, Kalas et al. (2015) detected a significant asymmetry of the outer disk ($>$ 200 au projected radius) via *Hubble Space Telescope/Advanced Camera for Surveys (HST/ACS)*, with a truncated fan structure on the southeast side and an extended linear morphology to the northwest. The outer giant planet HD 106906 b is a likely source of the perturbation, with the flybys playing a dynamical role in raising its periastron distance away from the central region close to the binary (Rodet et al. 2017; Nesvold et al. 2017; Nguyen et al. 2021).

4.4.2. HD 113556

We found an encounter between HD 113556 (F2V) and TYC 8674-2317-1 (K4) with $d_{ca} = 1.22^{+0.88}_{-0.53}$ pc at $t_{ca} = -1.55^{+0.46}_{-0.64}$ Myr. HD 113556 has Spitzer-detected 24 and 70 μ m infrared excesses (Chen et al. 2005, 2011a) in addition to the ALMA detection at 1.24 mm (Lieman-Sifry et al. 2016), which is unresolved. The flyby star, TYC 8674-2317-1, does not have reported thermal-IR excess from its *WISE* photometry, although it has not been targeted with either *Spitzer*, *Herschel*, or ALMA, all of which are more sensitive to cold dust at wider separations.

4.4.3. HD 114082

HD 114082 (F3V) had one encounter $2.85^{+0.16}_{-0.17}$ Myr ago with $d_{ca} = 0.87^{+0.36}_{-0.31}$ pc. The interaction has $\theta_{ca} = -13.91^{+3.96}_{-3.98}$ deg and a high relative velocity ($v_{rel} = 8.95 \pm 0.40$ km/s). Wahhaj et al. (2016) first resolved the HD 114082 disk in *H*-band scattered light as a ring with inner radius \sim 28 au and $i \sim 83^\circ$. Esposito et al. (2020) confirmed the ring structure in both *H*-band total intensity and polarized intensity images. They noted that dust scattered light

Table 1. Flyby events involving resolved or detected debris disks

Target star	Flyby star	d_0	d_{ca}	t_{ca}	θ_{ca}	v_{rel}	Ref
		(pc)	(pc)	(Myr)	(deg)	(km/s)	
HD 106906	HD 106444	$11.55^{+0.69}_{-0.68}$	$0.65^{+0.92}_{-0.40}$	$-3.49^{+0.90}_{-1.75}$	$5.90^{+1.77}_{-1.67}$	$3.22^{+1.10}_{-1.09}$	1
	HIP 59721	$11.89^{+0.64}_{-0.65}$	$0.71^{+0.18}_{-0.11}$	$-2.19^{+0.54}_{-1.03}$	$4.64^{+1.00}_{-1.16}$	$5.30^{+1.70}_{-1.69}$	
HD 113556	TYC 8674-2317-1	$7.03^{+0.47}_{-0.46}$	$1.22^{+0.88}_{-0.53}$	$-1.55^{+0.46}_{-0.64}$... †	$4.34^{+1.65}_{-1.45}$	2
HD 114082	HD 116402	$26.09^{+0.87}_{-0.86}$	$0.87^{+0.36}_{-0.31}$	$-2.85^{+0.16}_{-0.17}$	$-13.91^{+3.96}_{-3.98}$	$8.95^{+0.40}_{-0.40}$	1
HD 115600	TYC 8674-2317-1	$2.37^{+0.56}_{-0.54}$	$0.89^{+0.09}_{-0.06}$	$0.62^{+0.65}_{-0.26}$	$10.52^{+1.79}_{-1.69}$	$3.35^{+1.81}_{-1.79}$	1
HD 142315	HD 142705	$2.21^{+1.27}_{-0.53}$	$1.60^{+0.77}_{-0.77}$	$-0.26^{+0.62}_{-0.98}$... †	$2.70^{+2.52}_{-1.34}$	2
	UCAC4 336-078484	$1.93^{+1.10}_{-0.47}$	$1.36^{+0.50}_{-0.45}$	$-0.17^{+0.46}_{-0.79}$... †	$3.40^{+3.47}_{-2.02}$	
	HD 142097	$4.91^{+1.35}_{-1.26}$	$1.55^{+0.19}_{-0.12}$	$0.59^{+0.35}_{-0.22}$... †	$7.77^{+2.67}_{-2.59}$	
2M J16035767-2031055	2M J16053815-2039469	$5.24^{+1.24}_{-1.23}$	$0.52^{+0.29}_{-0.16}$	$-0.43^{+0.17}_{-0.39}$	$-11.52^{+29.51}_{-27.92}$	$11.37^{+5.81}_{-5.66}$	3
	RX J1603.9-2031B	$9.05^{+5.29}_{-4.91}$	$0.71^{+2.06}_{-0.48}$	$0.96^{+1.80}_{-1.23}$	$-11.65^{+33.98}_{-29.84}$	$6.29^{+5.68}_{-4.19}$	
2M J16042165-2130284	EPIC 204548337	$1.98^{+1.35}_{-0.73}$	$1.06^{+1.03}_{-0.69}$	$0.33^{+0.56}_{-0.59}$	$-27.59^{+86.39}_{-47.42}$	$2.86^{+2.44}_{-1.18}$	4
2M J16064794-1841437	HD 144925	$18.19^{+1.72}_{-1.72}$	$0.73^{+0.28}_{-0.24}$	$-1.32^{+0.26}_{-0.40}$	$-30.90^{+1.21}_{-0.83}$	$13.46^{+2.96}_{-2.95}$	5
HD 145718	HD 145467	$14.04^{+2.11}_{-2.05}$	$1.16^{+1.36}_{-0.60}$	$-2.31^{+0.63}_{-1.03}$	$-20.56^{+1.87}_{-1.84}$	$5.96^{+1.86}_{-1.82}$	5
	2M J16120920-2247504	$11.14^{+2.21}_{-2.17}$	$1.04^{+0.63}_{-0.33}$	$-1.96^{+0.63}_{-1.25}$	$-18.17^{+2.11}_{-1.81}$	$5.50^{+2.08}_{-2.07}$	
	BD-21 4301	$18.21^{+2.57}_{-2.58}$	$1.30^{+1.54}_{-0.79}$	$-1.20^{+0.36}_{-0.73}$	$-19.15^{+1.51}_{-1.40}$	$14.66^{+5.61}_{-5.57}$	
	Gaia DR2 6242198746659039872	$8.66^{+2.10}_{-2.05}$	$1.12^{+0.38}_{-0.48}$	$-1.03^{+0.48}_{-1.26}$	$-21.61^{+2.01}_{-2.68}$	$7.32^{+4.78}_{-4.41}$	
	2M J16125889-2245202	$2.86^{+2.20}_{-1.69}$	$0.93^{+0.96}_{-0.18}$	$0.15^{+0.69}_{-0.83}$	$8.91^{+31.88}_{-21.88}$	$4.70^{+4.93}_{-2.99}$	
HD 146897	HD 146416	$2.00^{+1.16}_{-0.57}$	$0.65^{+0.61}_{-0.43}$	$-0.44^{+0.31}_{-0.33}$	$4.23^{+4.37}_{-4.34}$	$4.08^{+0.33}_{-0.32}$	1
	HD 147083	$1.82^{+1.59}_{-1.03}$	$0.58^{+0.46}_{-0.13}$	$0.51^{+1.34}_{-1.09}$	$5.19^{+10.26}_{-12.69}$	$1.88^{+1.76}_{-1.21}$	
	HD 146743	$6.62^{+1.27}_{-1.27}$	$1.12^{+0.53}_{-0.38}$	$1.63^{+0.49}_{-0.39}$	$-2.26^{+4.36}_{-4.20}$	$3.91^{+0.75}_{-0.75}$	

NOTE—† The target star disks have not been spatially resolved.

References—(1) Esposito et al. 2020; (2) Lieman-Sifry et al. 2016; (3) Barenfeld et al. 2016, 2017; (4) Mayama et al. 2012; (5) Ansdell et al. 2020

was 1.5–1.8 times brighter on the west side of the disk compared to the east out to a radius of 1.2". Deep optical images obtained with HST/STIS have detected the disk ansae to $\sim 5.4''$ (520 au) radius from the star but a significant asymmetry in brightness or structure between the two ansae is not evident (T. Esposito, priv. comm.). The flyby star, HD 116402 (G3V), does not have a measured infrared excess, and there are no published high-contrast imaging data searching for a debris disk around this star.

4.4.4. HD 115600

We calculated that HD 115600 (F2IV/V) will encounter TYC 8674-2317-1 with $t_{ca} = 0.62^{+0.65}_{-0.26}$ Myr and $d_{ca} = 0.89^{+0.09}_{-0.06}$ pc. Though t_{ca} is in the future, a closest approach at the present epoch is within the 3- σ uncertainty. The closest approach angle is $\theta_{ca} = 10.52^{+1.79}_{-1.69}$ deg. Previous GPI (Currie et al. 2015) and SPHERE (Gibbs et al. 2019) detections of the HD 115600 disk show a ring of dust at roughly 46 au radius. Currie et al. (2015) report a possible (2 σ) stellocentric offset that could be attributed to an eccentric planet (Thilliez & Maddison 2017), but the offset was not confirmed

by Gibbs et al. (2019). An optical image with HST/STIS over a wider field of view does not detect the disk beyond $\sim 1.5''$ (164 au) radius (T. Esposito, priv. comm.) and shows no ring or spiral structures that would be evidence for a dynamical perturbation.

4.4.5. HD 142315

HD 142315 (B9V) had very recent encounters with HD 142705 (A0V) at $d_{ca} = 1.60 \pm 0.77$ pc and $t_{ca} = -0.26^{+0.62}_{-0.98}$ Myr and UCAC4 336-078484 (M0.5) at $d_{ca} = 1.36^{+0.50}_{-0.45}$ pc and $t_{ca} = -0.17^{+0.46}_{-0.79}$ Myr; given the uncertainties, these two flyby events are at their closest distances at the present epoch. Figure 9 (panel e) shows that HD 142705 and UCAC4 336-078484 have very similar posterior distributions in the d_{ca} - t_{ca} space, suggesting that the two stars share similar space velocities and may be a gravitationally-bound wide binary. These two stars are separated on the sky by 0.20 deg, and have a three-dimensional separation of $1.40^{+1.36}_{-0.75}$ pc. At this separation, the escape velocity for the two stars assuming a circular orbit is $0.11^{+0.05}_{-0.03}$ km s⁻¹. From their astrometry and radial velocities, we measured a

relative velocity of $3.28_{-2.26}^{+3.52}$ km s⁻¹. When considering the uncertainties, this is not significantly different from the predicted escape velocity. More precise radial velocity measurements of the two stars are required in order to refine the estimate of their relative velocities. HD 142315 is also predicted to encounter HD 142097 (A5V) in the future at $d_{ca} = 1.55_{-0.12}^{+0.19}$ pc and $t_{ca} = 0.59_{-0.22}^{+0.35}$ Myr.

4.4.6. 2MASS J16035767-2031055 (J1603-2031)

We calculated that the K0 star 2MASS J16035767-2031055 had a very recent close approach with 2MASS J16053815-2039469 (M0) at $t_{ca} = -0.43_{-0.39}^{+0.17}$ Myr with a close approach distance at $d_{ca} = 0.52_{-0.16}^{+0.29}$ pc. We also identified that the K-star will have another close approach with RX J1603.9-2031B at $t_{ca} = 0.96_{-1.23}^{+1.80}$ Myr with a close approach distance of $d_{ca} = 0.71_{-0.48}^{+2.06}$ pc. Incorporating the position angle and inclination derived by Barenfeld et al. (2017) based on the ALMA continuum detection, we computed the flyby angle of the two events to be $\theta_{ca} = -11.52_{-27.92}^{+29.51}$ deg and $\theta_{ca} = -11.65_{-29.84}^{+33.98}$ deg, respectively. The flyby angle is basically unconstrained due to the the large ($\sim 30\%$) uncertainties in the fitted disk orientation. Additionally, Garufi et al. (2020) carries out observations on this star in *H*-band using SPHERE but reports a non-detection of any disk in scattered light.

J1603-2031 (also catalogued as RX J1603.9-2031A) and RX J1603.9-2031B were originally paired by Köhler et al. (2000), but their relative velocities are not consistent with them being gravitationally-bound. RX J1603.9-2031B is itself known to be a binary of two stars with similar magnitudes on a 53-year orbit (Tokovinin & Briceño 2018). The RV semi-amplitude of their assumed orbit is approximately 3.6 km s⁻¹. While this is larger than the uncertainties on the radial velocity measurement used for the analysis presented here, the measured velocity of the blended spectrum may not be significantly affected by binary motion due to the similar magnitudes of both components. A joint fit of the astrometry presented in Tokovinin & Briceño (2018) and radial velocity measurements where the two stars are spectrally resolved will be needed to determine the systemic velocity, refining the trajectory of this binary relative to J1603-2031.

4.4.7. 2MASS J16042165-2130284 (J1604-2130)

This K2 star will encounter the M1 star EPIC 204548337 (2MASS J16032787-2153155) with $d_{ca} = 1.22_{-0.53}^{+0.88}$ pc at $t_{ca} = 0.33_{-0.59}^{+0.56}$ Myr. Given the uncertainties in t_{ca} the closest approach epoch is near the present time and the current separation between the two stars is shown in Table 1. J1604-2130 hosts one of the largest disks in Upper Scorpius subgroup, appearing as a face-on dust and gas ring between roughly 15 and 300 au radius in thermal emission (Mathews et al. 2012; Zhang et al. 2014; Barenfeld et al. 2016; Dong et al. 2017) and scattered light (Mayama et al. 2012; Pinilla

et al. 2015, 2018). The median close approach angle is calculated to be $-27.59_{-47.42}^{+86.39}$ (Table 1). However, due to the bimodality of the posterior distribution of the close approach angle as displayed in panel (g) of Fig.9, we divided the distribution at $\theta_{ca} = 0^\circ$ and calculated the median of each section to be $52.46_{-30.30}^{+15.75}$ deg and $-64.89_{-14.05}^{+34.18}$ deg, which suggests that the flyby of EPIC 204548337 is nearly perpendicular to the disk plane. The azimuthal structure of the dust ring has a rotating deficit of scattered light that can be explained as shadowing by optically thick clumps orbiting within an inner dust disk. The existence of a clumpy inner disk misaligned with respect to the outer disk is supported by the observation of aperiodic photometric dips (Ansdell et al. 2016). Future work is needed to investigate if EPIC 204548337 plays a dynamical role in misaligning the outer disk relative to the inner disk (e.g., Kraus et al. 2020; Ginski et al. 2021).

4.4.8. 2MASS J16064794-1841437 (J1606-1841)

J1606-1841 (M0.0e) has an ALMA-resolved disk with $i = 55.5_{-0.1}^{+0.1}$ deg and PA= 20_{-1}^{+1} deg (Ansdell et al. 2020). The bi-lobed thermal emission map suggests a narrow ring-like structure. The flyby star HD 144295 (A0V) came within 0.7 R_H (Table 5) at $t_{ca} = -1.32_{-0.40}^{+0.26}$ Myr. The high relative velocity $v_{rel} = 13.46$ km/s (Table 1) makes it unlikely that the disk was significantly perturbed by the encounter. On the other hand, HD 144295 (HIP 79124) is a triple stellar system (Asensio-Torres et al. 2019; Ruane et al. 2019) that needs future characterization to improve the determination of the systemic velocity.

4.4.9. HD 145718

In Table 1 this A5 star it is distinguished by having a total of five flybys, all within ~ 2.5 million years. The flyby of 2MASS J16125889-2245202 (M0) has the smallest d_{ca} (0.93 pc), corresponding to 0.65 R_H (Table 5). Ansdell et al. (2020) report that HD 145718 has an ALMA-resolved disk with PA= 1_{-1}^{+1} deg and $i = 70.4_{-1.2}^{+1.2}$ deg. The inner circumstellar disk was resolved using VLTI GRAVITY in *K*-band, giving PA= 2_{+2}^{-2} deg and $i = 71.9_{-1.2}^{+1.2}$ (Gravity Collaboration et al. 2019). It was also resolved with VLTI PIONEER in *H*-band (Kluska et al. 2020), giving PA= -3_{-4}^{+4} deg and $i = 48_{-3}^{+3}$ deg. The main discrepancy is in the determination of disk inclination. For the purpose of calculating the encounter geometry, we adopt the values given by Ansdell et al. (2020). We note that the posterior distribution of the close approach angle with 2MASS J16125889-2245202 is bimodal—this is likely due to the fact that both stars' RV measurements are not certain about the direction of the line-of-sight motion. Therefore, we divided the distributions at $\theta_{ca} = 18^\circ$ into two sections and calculated the median of each section to be $33.64_{-7.98}^{+22.34}$ deg and $-10.22_{-4.23}^{+10.67}$ deg, respectively.

4.4.10. *HD 146897*

We find three flybys for HD 146897 (F2/F3V; HIP 79977), two in the recent past or present, and one in the future. HD 146897 had a close encounter with HD 146416 (B9V) at $t_{ca} = -0.44^{+0.31}_{-0.33}$ Myr and $d_{ca} = 0.65^{+0.61}_{-0.43}$ pc. The flyby is nearly coplanar with the debris disk ($\theta_{ca} = 4.23^{+4.37}_{-4.34}$ deg) which was first resolved in scattered light by [Thalmann et al. \(2013\)](#). [Goebel et al. \(2018\)](#) measured a brightness asymmetry along the midplane in images obtained with Subaru SCEXAO/CHARIS. This asymmetry is also seen in GPI images ([Esposito et al. 2020](#)) and extends to $>6''$ (789 au) radius in optical HST/STIS images ([Kalas et al. 2020](#)).

HD 146897 also has a close encounter with HD 147083 (A7III/IV) in the future or present with $t_{ca} = 0.51^{+1.34}_{-1.09}$ Myr, $d_{ca} = 0.58^{+0.46}_{-0.13}$ pc. The closest approach angle is $\theta_{ca} = 5.19^{+10.26}_{-12.69}$ deg. The error bar on θ_{ca} is large compared to the other flyby events because of the large uncertainty in the radial velocity of the flyby star.

Lastly, HD 146897 will possibly encounter HD 146743 (F3V) at $t_{ca} = 1.63^{+0.50}_{-0.39}$ Myr and $d_{ca} = 1.12^{+0.53}_{-0.38}$ pc. However, it is unlikely this encounter will affect the current disk morphology given the large closest approach distance.

5. POTENTIAL ENCOUNTERS IN UPPER SCORPIUS SUBGROUP

There are 1341 stars in the USCO sample that do not have RV measurement. We also attempted to identify potential close approaches between these stars and those that have RV measurements. While we cannot confidently determine which of these stars will have experienced a flyby event in the past, we can identify candidate encounters to motivate future radial velocity measurements of these stars to better understand their kinematics. For each pair of stars (let the one with RV measurement be star A and the other be star B), we sampled the 6D space position and motion of star A derived from *Gaia* astrometry and radial velocities, and the five known astrometric parameters of star B with 10^5 trials using the method in Section 3.1. For star B the radial velocity was fixed at a constant value, allowing us to identify candidate flyby events assuming this velocity. We repeated this exercise for radial velocities consistent with the distribution of other Upper Sco members ($-5 \pm 4 \text{ km s}^{-1}$; ([Gagné et al. 2018](#))), changing the radial velocity from -21 km s^{-1} to 11 km s^{-1} (-4σ to $+4\sigma$) in steps of 0.01 km s^{-1} .

Flyby events identified from this analysis that had $t_{CA} < 0$ Myr and where the radial velocity of star B was within the 1σ range of the distribution of Upper Sco members were selected as candidate flyby events within the USCO sample. Overall, we identified 30 potential close encounters and 224 potential encounters. The distribution of these candidate events in terms of closest approach time and distance is

shown in Figure 10, and a complete listing is given in Table 7.

Of these candidate encounters, four involve three stars with a measured IR excess in [Cotten & Song \(2016\)](#); HD 144587, HD 146069, and HD 145631 that has two candidate encounters. The paucity of excess stars within this sample is not surprising; many of these stars have only recently been identified as members of the Upper Sco subgroup. Of these three, only HD 144587 has been observed by a high-contrast imager to search for polarized emission from circumstellar material, but no detection was reported ([Uyama et al. 2017](#)). All of the stars have been the subject of adaptive optics searches for stellar companions. HD 145631 was resolved as a hierarchical triple system consisting of an F-type primary and at 191 au two K-type companions with a projected separation of 7.3 au ([Lafrenière et al. 2014](#)). It is not known what effect these companions are having on the morphology of the disk as it has not yet been spatially resolved.

6. CONCLUSION

Using astrometry from *Gaia* and radial velocities from a combination of literature sources, we searched for close stellar flybys within the Scorpius-Centaurus OB2 association. We calculated the closest approach distance and the time at which the close approaches take place for two samples of stars. The first consisted of 462 stars spanning all three subgroups of Sco-Cen whose membership were assessed primarily from *Hipparcos* astrometry (e.g., [de Zeeuw et al. 1999](#)), while the second contained 219 stars within the Upper Sco subgroup identified from a more recent analysis of *Gaia DR2* astrometry ([Luhman & Esplin 2020](#)). We identified 12 past close encounters (defined as one star entering the half hill sphere radius of another), and 12 future close encounters amongst the first sample, and 37 more distant encounters. Amongst the Upper Sco sample, we identified 36 past close encounters, 18 future close encounters, and 106 more distant encounters. We also searched for candidate flyby events involving the Upper Sco sample members that do not yet have radial velocity measurements. We identified 41 candidate close encounters given simulated radial velocities consistent with the measured distribution of other Upper Sco members ([Gagné et al. 2018](#)).

Motivated by theoretical work exploring the interaction between stellar flybys and the evolution of exoplanetary system architectures, we cross-matched the flyby events identified within this work with catalogues of stars within Sco-Cen that have measured infrared-excesses ([Cotten & Song 2016](#)), indicative of the presence of circumstellar material. For the subset of stars with an infrared excess we searched the literature for spatially resolved detections of these disks from which their geometry can be measured. A total of 10 stars with at least one identified flyby event have debris disks that

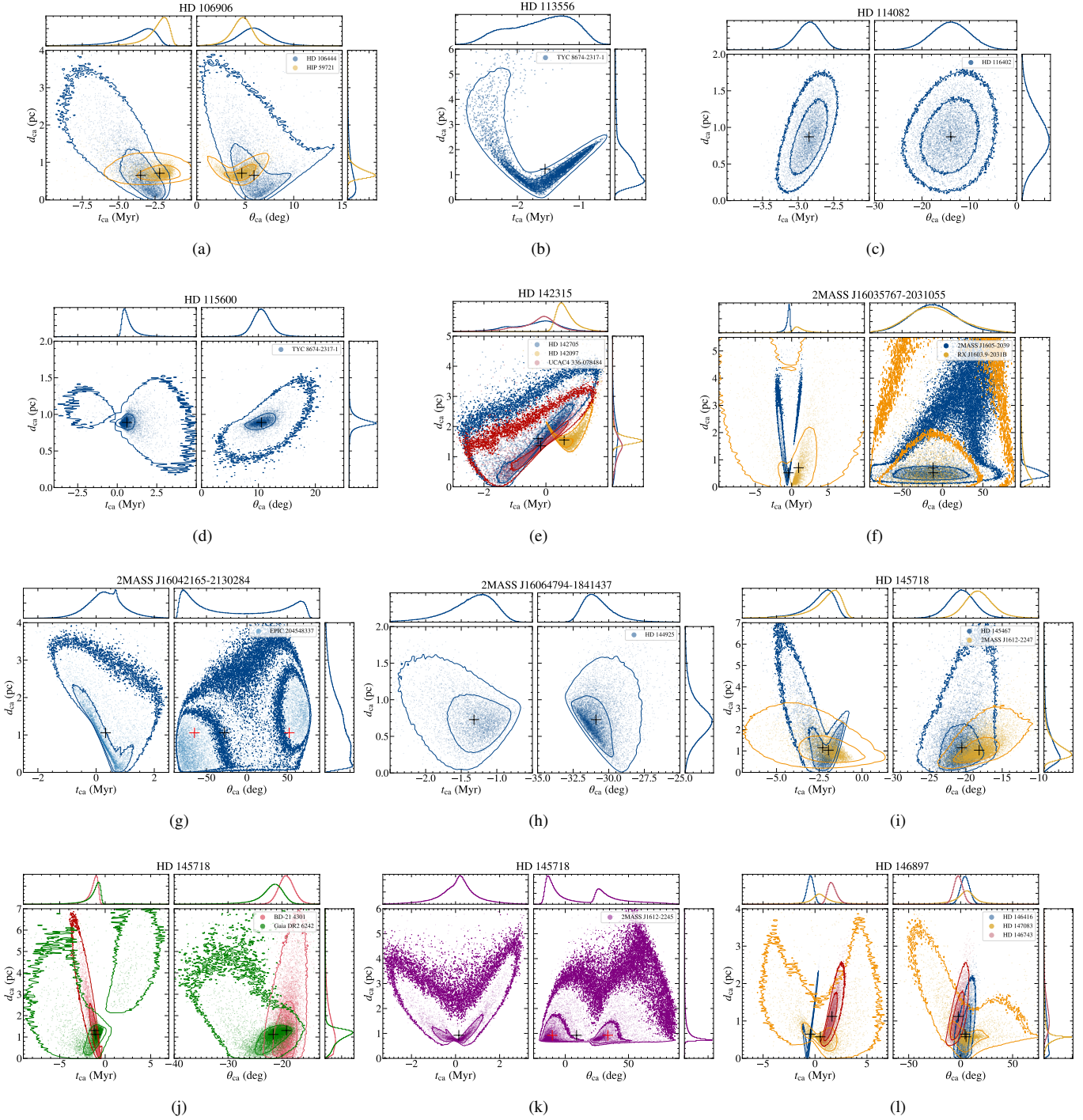


Figure 9. Closest approach distance as a function of closest approach time and closest approach angle for each of the flyby events involving detected debris disks. The crosses represent the median values of MC outputs; if the posterior distribution is bimodal, the median about each mode is marked by a red cross. The contours represent the 1σ and 2σ credible regions.

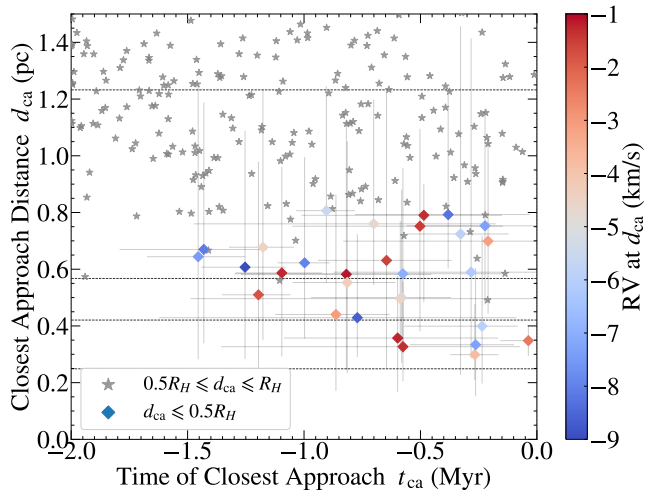


Figure 10. The potential close approaches that would have happened within the USCO subgroup by simulating the effect of perfectly knowing the RV of stars without RV measurement. The dotted lines mark the 1st-, 5th-, 10th-, and 50th-percentiles of the distribution of the separation of stars within the sample.

have been resolved either in scattered light from ground or space-based instrumentation, or detected at sub-millimeter wavelengths with ALMA. In one case, for HD 106906, the disk exhibits a strong brightness asymmetry (Kalas et al. 2015), but it is likely that this is caused by the orbiting planetary-mass companion (Bailey et al. 2014; Nguyen et al. 2021) rather than a direct interaction between the disk and the two flyby stars. For the remaining targets the existing evidence does not show significantly disturbed morphologies that could be caused by a flyby of another star.

Our incomplete census of the full Sco-Cen association limited the analysis presented here to the more massive stars ($> 1 M_{\odot}$) for two of the three subgroups. A more exhaustive search for flyby events can be undertaken when the membership of the three subgroups are re-assessed using data from current and future *Gaia* data releases. Another significant limitation is the precision of the radial velocity measurements

for many of the stars within our sample; a large uncertainty in the radial velocity at the current epoch significantly hampers our ability to predict the relative positions and velocities of pairs of stars within the cluster at earlier times. Future *Gaia* data releases will contain radial velocity measurements for many more of the cluster members than used in this study, but at a relatively low precision ($\sim 1 \text{ km s}^{-1}$). In order to accurately trace back the motions of the cluster members to confidently determine which pairs of stars experienced a close encounter in the past, precision radial velocities are needed in conjunction with the precision astrometry provided by *Gaia*. With these data, we will be able investigate more interesting and stronger dynamical interactions between flyby stars and debris disks to provide empirical evidence of the impact of stellar flybys on the evolution of planetary systems.

ACKNOWLEDGMENTS

We thank the anonymous referees for their comments that helped to improve the quality of this manuscript. The first author also thanks Eugene Chiang, Fanghui Wan, and Tianqi Wei for the valuable discussions and/or support regarding the work. This work is supported by NSF AST-1518332, NASA NNX15AC89G and NNX15AD95G/NEXSS. This work benefited from NASA’s Nexus for Exoplanet System Science (NEXSS) research coordination network sponsored by NASA’s Science Mission Directorate. This research has made use of the SIMBAD database and the VizieR catalogue access tool, both operated at the CDS, Strasbourg, France. This work has made use of data from the European Space Agency (ESA) mission *Gaia* (<https://www.cosmos.esa.int/gaia>), processed by the *Gaia* Data Processing and Analysis Consortium (DPAC, <https://www.cosmos.esa.int/web/gaia/dpac/consortium>). Funding for the DPAC has been provided by national institutions, in particular the institutions participating in the *Gaia* Multilateral Agreement.

REFERENCES

- Ansdell, M., Gaidos, E., Williams, J. P., et al. 2016, *MNRAS*, 462, L101, doi: [10.1093/mnras/slw140](https://doi.org/10.1093/mnras/slw140)
- Ansdell, M., Gaidos, E., Hedges, C., et al. 2020, *MNRAS*, 492, 572, doi: [10.1093/mnras/stz3361](https://doi.org/10.1093/mnras/stz3361)
- Ardila, D. R., Lubow, S. H., Golimowski, D. A., et al. 2005, *ApJ*, 627, 986, doi: [10.1086/430395](https://doi.org/10.1086/430395)
- Asensio-Torres, R., Currie, T., Janson, M., et al. 2019, *A&A*, 622, A42, doi: [10.1051/0004-6361/201834688](https://doi.org/10.1051/0004-6361/201834688)
- Augereau, J. C., & Papaloizou, J. C. B. 2004, *A&A*, 414, 1153, doi: [10.1051/0004-6361:20031622](https://doi.org/10.1051/0004-6361:20031622)
- Bailer-Jones, C. A. L., Rybizki, J., Andrae, R., & Foesneau, M. 2018, *A&A*, 616, A37, doi: [10.1051/0004-6361/201833456](https://doi.org/10.1051/0004-6361/201833456)
- Bailey, V., Meshkat, T., Reiter, M., et al. 2014, *ApJL*, 780, L4, doi: [10.1088/2041-8205/780/1/L4](https://doi.org/10.1088/2041-8205/780/1/L4)
- Barenfeld, S. A., Carpenter, J. M., Ricci, L., & Isella, A. 2016, *ApJ*, 827, 142, doi: [10.3847/0004-637X/827/2/142](https://doi.org/10.3847/0004-637X/827/2/142)
- Barenfeld, S. A., Carpenter, J. M., Sargent, A. I., Isella, A., & Ricci, L. 2017, *ApJ*, 851, 85, doi: [10.3847/1538-4357/aa989d](https://doi.org/10.3847/1538-4357/aa989d)
- Budding, E., Butland, R., & Blackford, M. 2015, *MNRAS*, 448, 3784, doi: [10.1093/mnras/stv234](https://doi.org/10.1093/mnras/stv234)

- Cabrit, S., Pety, J., Pésenti, N., & Dougados, C. 2006, *A&A*, 452, 897, doi: [10.1051/0004-6361:20054047](https://doi.org/10.1051/0004-6361:20054047)
- Chen, C. H., Jura, M., Gordon, K. D., & Blaylock, M. 2005, *ApJ*, 623, 493, doi: [10.1086/428607](https://doi.org/10.1086/428607)
- Chen, C. H., Mamajek, E. E., Bitner, M. A., et al. 2011a, *ApJ*, 738, 122, doi: [10.1088/0004-637X/738/2/122](https://doi.org/10.1088/0004-637X/738/2/122)
- . 2011b, *ApJ*, 738, 122, doi: [10.1088/0004-637X/738/2/122](https://doi.org/10.1088/0004-637X/738/2/122)
- Choi, J., Dotter, A., Conroy, C., et al. 2016, *ApJ*, 823, 102, doi: [10.3847/0004-637X/823/2/102](https://doi.org/10.3847/0004-637X/823/2/102)
- Cotten, T. H., & Song, I. 2016, *ApJS*, 225, 15, doi: [10.3847/0067-0049/225/1/15](https://doi.org/10.3847/0067-0049/225/1/15)
- Cuello, N., Dipierro, G., Mentiplay, D., et al. 2019, *MNRAS*, 483, 4114, doi: [10.1093/mnras/sty3325](https://doi.org/10.1093/mnras/sty3325)
- Cuello, N., Louvet, F., Mentiplay, D., et al. 2020, *MNRAS*, 491, 504, doi: [10.1093/mnras/stz2938](https://doi.org/10.1093/mnras/stz2938)
- Currie, T., Lisse, C. M., Kuchner, M., et al. 2015, *ApJL*, 807, L7, doi: [10.1088/2041-8205/807/1/L7](https://doi.org/10.1088/2041-8205/807/1/L7)
- Dahm, S. E., Slesnick, C. L., & White, R. J. 2012, *ApJ*, 745, 56, doi: [10.1088/0004-637X/745/1/56](https://doi.org/10.1088/0004-637X/745/1/56)
- Damiani, F., Prisinzano, L., Pillitteri, I., Micela, G., & Sciortino, S. 2019, *A&A*, 623, A112, doi: [10.1051/0004-6361/201833994](https://doi.org/10.1051/0004-6361/201833994)
- De Rosa, R. J., Dawson, R., & Nielsen, E. L. 2020, *A&A*, 640, A73, doi: [10.1051/0004-6361/202038496](https://doi.org/10.1051/0004-6361/202038496)
- De Rosa, R. J., & Kalas, P. 2019, *AJ*, 157, 125, doi: [10.3847/1538-3881/ab0109](https://doi.org/10.3847/1538-3881/ab0109)
- de Zeeuw, P. T., Hoogerwerf, R., de Bruijne, J. H. J., Brown, A. G. A., & Blaauw, A. 1999, *AJ*, 117, 354, doi: [10.1086/300682](https://doi.org/10.1086/300682)
- Desidera, S., Covino, E., Messina, S., et al. 2015, *A&A*, 573, A126, doi: [10.1051/0004-6361/201323168](https://doi.org/10.1051/0004-6361/201323168)
- Dong, R., van der Marel, N., Hashimoto, J., et al. 2017, *ApJ*, 836, 201, doi: [10.3847/1538-4357/aa5abf](https://doi.org/10.3847/1538-4357/aa5abf)
- Dotter, A. 2016, *ApJS*, 222, 8, doi: [10.3847/0067-0049/222/1/8](https://doi.org/10.3847/0067-0049/222/1/8)
- Duflot, M., Figon, P., & Meyssonnier, N. 1995, *A&AS*, 114, 269
- Duncan, M., Quinn, T., & Tremaine, S. 1987, *AJ*, 94, 1330, doi: [10.1086/114571](https://doi.org/10.1086/114571)
- ESA. 1997, *The Hipparcos and Tycho Catalogues*, ESA SP-1200
- Esposito, T. M., Kalas, P., Fitzgerald, M. P., et al. 2020, *arXiv e-prints*, arXiv:2004.13722. <https://arxiv.org/abs/2004.13722>
- Evans, D. S. 1967, in *IAU Symposium*, Vol. 30, *Determination of Radial Velocities and their Applications*, ed. A. H. Batten & J. F. Heard, 57
- Gagné, J., Mamajek, E. E., Malo, L., et al. 2018, *ApJ*, 856, 23, doi: [10.3847/1538-4357/aaae09](https://doi.org/10.3847/1538-4357/aaae09)
- Gaia Collaboration, Brown, A. G. A., Vallenari, A., et al. 2018, *A&A*, 616, A1, doi: [10.1051/0004-6361/201833051](https://doi.org/10.1051/0004-6361/201833051)
- Garufi, A., Avenhaus, H., Pérez, S., et al. 2020, *A&A*, 633, A82, doi: [10.1051/0004-6361/201936946](https://doi.org/10.1051/0004-6361/201936946)
- Gibbs, A., Wagner, K., Apai, D., et al. 2019, *AJ*, 157, 39, doi: [10.3847/1538-3881/aaf1bd](https://doi.org/10.3847/1538-3881/aaf1bd)
- Ginski, C., Facchini, S., Huang, J., et al. 2021, *ApJL*, 908, L25, doi: [10.3847/2041-8213/abdf57](https://doi.org/10.3847/2041-8213/abdf57)
- Goebel, S., Currie, T., Guyon, O., et al. 2018, *AJ*, 156, 279, doi: [10.3847/1538-3881/aaeb24](https://doi.org/10.3847/1538-3881/aaeb24)
- Gontcharov, G. A. 2006, *Astronomy Letters*, 32, 759, doi: [10.1134/S1063773706110065](https://doi.org/10.1134/S1063773706110065)
- Gravity Collaboration, Perraut, K., Labadie, L., et al. 2019, *A&A*, 632, A53, doi: [10.1051/0004-6361/201936403](https://doi.org/10.1051/0004-6361/201936403)
- Hartman, Z. D., & Lépine, S. 2020, *ApJS*, 247, 66, doi: [10.3847/1538-4365/ab79a6](https://doi.org/10.3847/1538-4365/ab79a6)
- Hills, J. G. 1981, *AJ*, 86, 1730, doi: [10.1086/113058](https://doi.org/10.1086/113058)
- . 1984, *AJ*, 89, 1559, doi: [10.1086/113659](https://doi.org/10.1086/113659)
- Ida, S., Larwood, J., & Burkert, A. 2000, *ApJ*, 528, 351, doi: [10.1086/308179](https://doi.org/10.1086/308179)
- Jiménez-Esteban, F. M., Solano, E., & Rodrigo, C. 2019, *AJ*, 157, 78, doi: [10.3847/1538-3881/aafacc](https://doi.org/10.3847/1538-3881/aafacc)
- Kalas, P., Deltorn, J.-M., & Larwood, J. 2001, *ApJ*, 553, 410, doi: [10.1086/320632](https://doi.org/10.1086/320632)
- Kalas, P., Esposito, T., Duchene, G., et al. 2020, in *American Astronomical Society Meeting Abstracts*, Vol. 235, *American Astronomical Society Meeting Abstracts #235*, 216.01
- Kalas, P., & Jewitt, D. 1995, *AJ*, 110, 794, doi: [10.1086/117565](https://doi.org/10.1086/117565)
- Kalas, P. G., Rajan, A., Wang, J. J., et al. 2015, *ApJ*, 814, 32, doi: [10.1088/0004-637X/814/1/32](https://doi.org/10.1088/0004-637X/814/1/32)
- Kaufmann, J. P., & Klippel, E. 1973, *A&A*, 27, 469
- Kennedy, G. M., Wyatt, M. C., Sibthorpe, B., et al. 2012, *MNRAS*, 421, 2264, doi: [10.1111/j.1365-2966.2012.20448.x](https://doi.org/10.1111/j.1365-2966.2012.20448.x)
- Kenyon, S. J., & Bromley, B. C. 2004, *Nature*, 432, 598, doi: [10.1038/nature03136](https://doi.org/10.1038/nature03136)
- Kharchenko, N. V., Scholz, R. D., Piskunov, A. E., Röser, S., & Schilbach, E. 2007, *Astronomische Nachrichten*, 328, 889, doi: [10.1002/asna.200710776](https://doi.org/10.1002/asna.200710776)
- Kley, W., & Nelson, R. P. 2012, *ARA&A*, 50, 211, doi: [10.1146/annurev-astro-081811-125523](https://doi.org/10.1146/annurev-astro-081811-125523)
- Kluska, J., Berger, J. P., Malbet, F., et al. 2020, *A&A*, 636, A116, doi: [10.1051/0004-6361/201833774](https://doi.org/10.1051/0004-6361/201833774)
- Kobayashi, H., Ida, S., & Tanaka, H. 2005, *Icarus*, 177, 246, doi: [10.1016/j.icarus.2005.02.017](https://doi.org/10.1016/j.icarus.2005.02.017)
- Köhler, R., Kunkel, M., Leinert, C., & Zinnecker, H. 2000, *A&A*, 356, 541
- Kordopatis, G., Gilmore, G., Steinmetz, M., et al. 2013, *AJ*, 146, 134, doi: [10.1088/0004-6256/146/5/134](https://doi.org/10.1088/0004-6256/146/5/134)
- Kraus, S., Kreplin, A., Young, A. K., et al. 2020, *Science*, 369, 1233, doi: [10.1126/science.aba4633](https://doi.org/10.1126/science.aba4633)
- Lafrenière, D., Jayawardhana, R., van Kerkwijk, M. H., Brandeker, A., & Janson, M. 2014, *ApJ*, 785, 47, doi: [10.1088/0004-637X/785/1/47](https://doi.org/10.1088/0004-637X/785/1/47)
- Lagrange, A. M., Langlois, M., Gratton, R., et al. 2016, *A&A*, 586, L8, doi: [10.1051/0004-6361/201527264](https://doi.org/10.1051/0004-6361/201527264)

- Larwood, J. D. 1997, *MNRAS*, 290, 490, doi: [10.1093/mnras/290.3.490](https://doi.org/10.1093/mnras/290.3.490)
- Larwood, J. D., & Kalas, P. G. 2001, *MNRAS*, 323, 402, doi: [10.1046/j.1365-8711.2001.04212.x](https://doi.org/10.1046/j.1365-8711.2001.04212.x)
- Lestrade, J. F., Morey, E., Lassus, A., & Phou, N. 2011, *A&A*, 532, A120, doi: [10.1051/0004-6361/201014730](https://doi.org/10.1051/0004-6361/201014730)
- Levato, H., Malaroda, S., Morrell, N., & Solivella, G. 1987, *ApJS*, 64, 487, doi: [10.1086/191204](https://doi.org/10.1086/191204)
- Levato, H., Malaroda, S., Morrell, N., Solivella, G., & Grosso, M. 1996, *A&AS*, 118, 231
- Levison, H. F., Duncan, M. J., Brasser, R., & Kaufmann, D. E. 2010, *Science*, 329, 187, doi: [10.1126/science.1187535](https://doi.org/10.1126/science.1187535)
- Lieman-Sifry, J., Hughes, A. M., Carpenter, J. M., et al. 2016, *ApJ*, 828, 25, doi: [10.3847/0004-637X/828/1/25](https://doi.org/10.3847/0004-637X/828/1/25)
- Luhman, K. L., & Esplin, T. L. 2020, arXiv e-prints, arXiv:2005.10128. <https://arxiv.org/abs/2005.10128>
- Luhman, K. L., & Mamajek, E. E. 2012, *ApJ*, 758, 31, doi: [10.1088/0004-637X/758/1/31](https://doi.org/10.1088/0004-637X/758/1/31)
- Malmberg, D., Davies, M. B., & Heggie, D. C. 2011, *MNRAS*, 411, 859, doi: [10.1111/j.1365-2966.2010.17730.x](https://doi.org/10.1111/j.1365-2966.2010.17730.x)
- Mamajek, E. E., Barenfeld, S. A., Ivanov, V. D., et al. 2015, *ApJL*, 800, L17, doi: [10.1088/2041-8205/800/1/L17](https://doi.org/10.1088/2041-8205/800/1/L17)
- Mason, B. D., Wycoff, G. L., Hartkopf, W. I., Douglass, G. G., & Worley, C. E. 2001, *AJ*, 122, 3466, doi: [10.1086/323920](https://doi.org/10.1086/323920)
- . 2020, *VizieR Online Data Catalog*, B/wds
- Mathews, G. S., Williams, J. P., & Ménard, F. 2012, *ApJ*, 753, 59, doi: [10.1088/0004-637X/753/1/59](https://doi.org/10.1088/0004-637X/753/1/59)
- Mathias, P., Gillet, D., & Crowe, R. 1991, *A&A*, 252, 245
- Mayama, S., Hashimoto, J., Muto, T., et al. 2012, *ApJL*, 760, L26, doi: [10.1088/2041-8205/760/2/L26](https://doi.org/10.1088/2041-8205/760/2/L26)
- Nesvold, E. R., Naoz, S., & Fitzgerald, M. P. 2017, *ApJL*, 837, L6, doi: [10.3847/2041-8213/aa61a7](https://doi.org/10.3847/2041-8213/aa61a7)
- Nguyen, M. M., De Rosa, R. J., & Kalas, P. 2021, *AJ*, 161, 22, doi: [10.3847/1538-3881/abc012](https://doi.org/10.3847/1538-3881/abc012)
- Oort, J. H. 1950, *BAN*, 11, 91
- Parker, R. J., & Quanz, S. P. 2012, *MNRAS*, 419, 2448, doi: [10.1111/j.1365-2966.2011.19911.x](https://doi.org/10.1111/j.1365-2966.2011.19911.x)
- Paxton, B., Bildsten, L., Dotter, A., et al. 2011, *ApJS*, 192, 3, doi: [10.1088/0067-0049/192/1/3](https://doi.org/10.1088/0067-0049/192/1/3)
- Paxton, B., Cantiello, M., Arras, P., et al. 2013, *ApJS*, 208, 4, doi: [10.1088/0067-0049/208/1/4](https://doi.org/10.1088/0067-0049/208/1/4)
- Pecaut, M. J., & Mamajek, E. E. 2013, *ApJS*, 208, 9, doi: [10.1088/0067-0049/208/1/9](https://doi.org/10.1088/0067-0049/208/1/9)
- . 2016, *MNRAS*, 461, 794, doi: [10.1093/mnras/stw1300](https://doi.org/10.1093/mnras/stw1300)
- Pfalzner, S., Bhandare, A., Vincke, K., & Lacerda, P. 2018, *ApJ*, 863, 45, doi: [10.3847/1538-4357/aad23c](https://doi.org/10.3847/1538-4357/aad23c)
- Pfalzner, S., Vogel, P., Scharwächter, J., & Olczak, C. 2005, *A&A*, 437, 967, doi: [10.1051/0004-6361:20042467](https://doi.org/10.1051/0004-6361:20042467)
- Pinilla, P., de Boer, J., Benisty, M., et al. 2015, *A&A*, 584, L4, doi: [10.1051/0004-6361/201526981](https://doi.org/10.1051/0004-6361/201526981)
- Pinilla, P., Benisty, M., de Boer, J., et al. 2018, *ApJ*, 868, 85, doi: [10.3847/1538-4357/aae824](https://doi.org/10.3847/1538-4357/aae824)
- Rasio, F. A., & Ford, E. B. 1996, *Science*, 274, 954, doi: [10.1126/science.274.5289.954](https://doi.org/10.1126/science.274.5289.954)
- Raymond, S. N., Armitage, P. J., & Gorelick, N. 2010, *ApJ*, 711, 772, doi: [10.1088/0004-637X/711/2/772](https://doi.org/10.1088/0004-637X/711/2/772)
- Reche, R., Beust, H., & Augereau, J. C. 2009, *A&A*, 493, 661, doi: [10.1051/0004-6361:200810419](https://doi.org/10.1051/0004-6361:200810419)
- Riedel, A. R., Alam, M. K., Rice, E. L., Cruz, K. L., & Henry, T. J. 2017, *ApJ*, 840, 87, doi: [10.3847/1538-4357/840/2/87](https://doi.org/10.3847/1538-4357/840/2/87)
- Rodet, L., Beust, H., Bonnefoy, M., et al. 2017, *A&A*, 602, A12, doi: [10.1051/0004-6361/201630269](https://doi.org/10.1051/0004-6361/201630269)
- Rodriguez, J. E., Loomis, R., Cabrit, S., et al. 2018, *ApJ*, 859, 150, doi: [10.3847/1538-4357/aac08f](https://doi.org/10.3847/1538-4357/aac08f)
- Rosotti, G. P., Dale, J. E., de Juan Ovelar, M., et al. 2014, *MNRAS*, 441, 2094, doi: [10.1093/mnras/stu679](https://doi.org/10.1093/mnras/stu679)
- Ruane, G., Ngo, H., Mawet, D., et al. 2019, *AJ*, 157, 118, doi: [10.3847/1538-3881/aafee2](https://doi.org/10.3847/1538-3881/aafee2)
- Song, I., Zuckerman, B., & Bessell, M. S. 2012, *AJ*, 144, 8, doi: [10.1088/0004-6256/144/1/8](https://doi.org/10.1088/0004-6256/144/1/8)
- Stickland, D. J., Sahade, J., & Henrichs, H. 1996, *The Observatory*, 116, 85
- Tamuz, O., Ségransan, D., Udry, S., et al. 2008, *A&A*, 480, L33, doi: [10.1051/0004-6361:20078737](https://doi.org/10.1051/0004-6361:20078737)
- Thackeray, A. D., & Hutchings, F. B. 1965, *MNRAS*, 129, 191, doi: [10.1093/mnras/129.2.191](https://doi.org/10.1093/mnras/129.2.191)
- Thalmann, C., Janson, M., Buenzli, E., et al. 2013, *ApJL*, 763, L29, doi: [10.1088/2041-8205/763/2/L29](https://doi.org/10.1088/2041-8205/763/2/L29)
- Thilliez, E., & Maddison, S. T. 2017, *MNRAS*, 464, 1434, doi: [10.1093/mnras/stw2427](https://doi.org/10.1093/mnras/stw2427)
- Tokovinin, A. 2018, *AJ*, 156, 194, doi: [10.3847/1538-3881/aadfe6](https://doi.org/10.3847/1538-3881/aadfe6)
- Tokovinin, A., & Briceño, C. 2018, *AJ*, 156, 138, doi: [10.3847/1538-3881/aad906](https://doi.org/10.3847/1538-3881/aad906)
- Torres, C. A. O., Quast, G. R., da Silva, L., et al. 2006, *A&A*, 460, 695, doi: [10.1051/0004-6361:20065602](https://doi.org/10.1051/0004-6361:20065602)
- Triaud, A. H. M. J., Collier Cameron, A., Queloz, D., et al. 2010, *A&A*, 524, A25, doi: [10.1051/0004-6361/201014525](https://doi.org/10.1051/0004-6361/201014525)
- Uyama, T., Hashimoto, J., Kuzuhara, M., et al. 2017, *AJ*, 153, 106, doi: [10.3847/1538-3881/153/3/106](https://doi.org/10.3847/1538-3881/153/3/106)
- Viana Almeida, P., Santos, N. C., Melo, C., et al. 2009, *A&A*, 501, 965, doi: [10.1051/0004-6361/200811194](https://doi.org/10.1051/0004-6361/200811194)
- Wahhaj, Z., Milli, J., Kennedy, G., et al. 2016, *A&A*, 596, L4, doi: [10.1051/0004-6361/201629769](https://doi.org/10.1051/0004-6361/201629769)
- Weinberger, A. J., Rich, R. M., Becklin, E. E., Zuckerman, B., & Matthews, K. 2000, *ApJ*, 544, 937, doi: [10.1086/317243](https://doi.org/10.1086/317243)
- Winter, A. J., Clarke, C. J., Rosotti, G., & Booth, R. A. 2018, *MNRAS*, 475, 2314, doi: [10.1093/mnras/sty012](https://doi.org/10.1093/mnras/sty012)
- Wright, N. J., & Mamajek, E. E. 2018, *MNRAS*, 476, 381, doi: [10.1093/mnras/sty207](https://doi.org/10.1093/mnras/sty207)

Zakamska, N. L., & Tremaine, S. 2004, AJ, 128, 869,
doi: [10.1086/422023](https://doi.org/10.1086/422023)

Zhang, K., Isella, A., Carpenter, J. M., & Blake, G. A. 2014, ApJ,
791, 42, doi: [10.1088/0004-637X/791/1/42](https://doi.org/10.1088/0004-637X/791/1/42)

APPENDIX

A. TABLES OF THE TWO SAMPLES AND ALL IDENTIFIED EVENTS

Table 2. RV measurements of Sco-Cen sample

Target	<i>Gaia</i> DR2 identifier	SpT	Mass (M_{\odot})	Subgroup	<i>Gaia</i> RV (km/s)	<i>Gaia</i> RV error (km/s)	RV (km/s)	RV error (km/s)	ref.
HD 103823	3463980463840622848	G2/3V	1.256	LCC	19.3	0.28	19.5	2.3	14
⋮	⋮	⋮	⋮	⋮	⋮	⋮	⋮	⋮	⋮

References—(1) Thackeray & Hutchings 1965; (2) Kaufmann & Klippel 1973; (3) Evans 1967; (4) Levato et al. 1987; (5) Mathias et al. 1991; (6) Levato et al. 1996; (7) Stickland et al. 1996; (8) Torres et al. 2006; (9) Gontcharov 2006; (10) Kharchenko et al. 2007; (11) Chen et al. 2011b; (12) Song et al. 2012; (13) Dahm et al. 2012; (14) Kordopatis et al. 2013; (15) Desidera et al. 2015; (16) Budding et al. 2015; (17) Riedel et al. 2017; (18) Tokovinin 2018; (19) Gaia Collaboration et al. 2018; (20) De Rosa & Kalas 2019.

NOTE—The full table will be available in the online version of the paper and on Vizier.

Table 3. RV measurements of USCO sample

Target	<i>Gaia</i> DR2 identifier	SpT	Mass (M_{\odot})	<i>Gaia</i> RV (km/s)	<i>Gaia</i> RV error (km/s)	RV (km/s)	RV error (km/s)	ref.
2MASS J15401546-1620577	6261607772589226496	...	12.971	-12.12	4.24	-12.12	4.24	8
⋮	⋮	⋮	⋮	⋮	⋮	⋮	⋮	⋮

References—(1) Levato et al. 1987; (2) Mathias et al. 1991; (3) Duflot et al. (1995); (4) Gontcharov 2006; (5) Kharchenko et al. 2007; (6) Chen et al. 2011b; (7) Dahm et al. 2012; (8) Gaia Collaboration et al. 2018

NOTE—The full table will be available in the online version of the paper and on Vizier

Table 4. Events identified from Sco-Cen sample

Star 1	Star 2	t_{ca} (Myr)	d_{ca} (pc)	d_{ca}/R_{HT}	d_{ca}/R_{HF}	Category	IR Excess?
2MASS J12143187-5110156	CD-50 6815	$0.02^{+0.30}_{-0.30}$	$0.18^{+0.40}_{-0.14}$	$0.17^{+0.36}_{-0.12}$	$0.14^{+0.31}_{-0.11}$	TF0.5	...
CD-48 8201	HD 116650	$-0.21^{+0.07}_{-0.09}$	$0.51^{+0.24}_{-0.28}$	$0.42^{+0.20}_{-0.23}$	$0.39^{+0.19}_{-0.22}$	TF0.5	...
HD 104231	HD 104125	$-0.61^{+0.26}_{-0.32}$	$0.24^{+0.28}_{-0.11}$	$0.18^{+0.21}_{-0.09}$	$0.16^{+0.18}_{-0.08}$	TF0.5	T
HD 106444	HIP 59721	$-0.09^{+0.32}_{-0.37}$	$0.08^{+0.16}_{-0.05}$	$0.06^{+0.12}_{-0.04}$	$0.06^{+0.13}_{-0.04}$	TF0.5	...
HD 106906	HD 106444	$-3.49^{+0.90}_{-1.75}$	$0.65^{+0.92}_{-0.40}$	$0.48^{+0.68}_{-0.30}$	$0.48^{+0.69}_{-0.30}$	TF0.5	T
HD 107821	TYC 8983-854-1	$0.42^{+0.22}_{-0.16}$	$0.56^{+0.20}_{-0.11}$	$0.37^{+0.13}_{-0.07}$	$0.45^{+0.16}_{-0.09}$	TF0.5	...
HD 110634	2MASS J12454884-5410583	$-0.94^{+0.14}_{-0.19}$	$0.62^{+0.14}_{-0.17}$	$0.45^{+0.10}_{-0.12}$	$0.49^{+0.11}_{-0.13}$	TF0.5	T
HD 145631	HD 145502	$0.34^{+0.49}_{-0.48}$	$0.64^{+0.46}_{-0.20}$	$0.39^{+0.28}_{-0.12}$	$0.27^{+0.20}_{-0.09}$	TF0.5	T
HD 146897	HD 146416	$-0.44^{+0.31}_{-0.33}$	$0.65^{+0.61}_{-0.43}$	$0.45^{+0.42}_{-0.30}$	$0.40^{+0.37}_{-0.27}$	TF0.5	T
HD 146897	HD 147083	$0.51^{+1.34}_{-1.09}$	$0.58^{+0.46}_{-0.13}$	$0.40^{+0.32}_{-0.09}$	$0.39^{+0.31}_{-0.09}$	TF0.5	T
HD 147010	HD 147104	$0.19^{+0.27}_{-0.14}$	$0.32^{+0.43}_{-0.06}$	$0.19^{+0.27}_{-0.04}$	$0.20^{+0.27}_{-0.04}$	TF0.5	...
TYC 7344-788-1	2MASS J16265700-3032232	$-0.01^{+0.31}_{-0.31}$	$0.37^{+0.63}_{-0.27}$	$0.31^{+0.53}_{-0.24}$	$0.32^{+0.55}_{-0.24}$	TF0.5	...
2MASS J15334052-3917467	HD 138204	$0.01^{+0.13}_{-0.08}$	$0.72^{+0.02}_{-0.02}$	$0.93^{+0.03}_{-0.02}$	$0.48^{+0.01}_{-0.01}$	F0.5	...
HD 145554	HD 145502	$0.06^{+0.45}_{-0.46}$	$0.92^{+1.38}_{-0.64}$	$0.56^{+0.85}_{-0.39}$	$0.39^{+0.60}_{-0.28}$	F0.5	T
CD-62 657	TYC 8983-564-1	$-1.06^{+0.41}_{-0.88}$	$1.18^{+0.27}_{-0.33}$	$0.92^{+0.21}_{-0.26}$	$0.94^{+0.21}_{-0.26}$	TF	...
CPD-64 1859	2MASS J12205449-6457242	$0.11^{+0.35}_{-0.42}$	$0.84^{+1.08}_{-0.58}$	$0.68^{+0.87}_{-0.46}$	$0.69^{+0.89}_{-0.48}$	TF	...
HD 104021	CPD-52 5025	$0.15^{+0.16}_{-0.15}$	$0.90^{+0.08}_{-0.11}$	$0.63^{+0.06}_{-0.07}$	$0.75^{+0.07}_{-0.09}$	TF	...
HD 105613	HD 104900	$-0.24^{+0.08}_{-0.15}$	$1.49^{+0.20}_{-0.35}$	$1.00^{+0.13}_{-0.23}$	$0.91^{+0.12}_{-0.21}$	TF	T
HD 105857	HD 106218	$-0.13^{+0.05}_{-0.06}$	$1.18^{+0.02}_{-0.02}$	$0.79^{+0.01}_{-0.01}$	$0.87^{+0.01}_{-0.01}$	TF	T
HD 106036	HD 106538	$-1.10^{+0.22}_{-0.34}$	$0.76^{+0.17}_{-0.14}$	$0.50^{+0.11}_{-0.09}$	$0.58^{+0.13}_{-0.10}$	TF	T
HD 106473	[SZB2012]9	$-0.61^{+0.20}_{-0.19}$	$1.08^{+1.24}_{-0.48}$	$0.75^{+0.86}_{-0.33}$	$0.88^{+1.01}_{-0.39}$	TF	...
HD 106906	HIP 59721	$-2.19^{+0.54}_{-1.03}$	$0.71^{+0.18}_{-0.11}$	$0.53^{+0.13}_{-0.08}$	$0.55^{+0.14}_{-0.09}$	TF	T
HD 107696	HD 106490	$0.61^{+0.28}_{-0.28}$	$1.72^{+0.90}_{-0.61}$	$0.91^{+0.48}_{-0.32}$	$0.73^{+0.38}_{-0.26}$	TF	...
HD 108501	TYC 8983-854-1	$-0.17^{+0.29}_{-0.35}$	$1.04^{+0.24}_{-0.06}$	$0.66^{+0.15}_{-0.04}$	$0.85^{+0.20}_{-0.05}$	TF	...
HD 109197	CPD-53 5235	$1.80^{+0.46}_{-0.32}$	$0.83^{+0.66}_{-0.40}$	$0.55^{+0.44}_{-0.26}$	$0.66^{+0.52}_{-0.31}$	TF	...
HD 109808	HD 110461	$-0.01^{+0.10}_{-0.10}$	$1.42^{+0.49}_{-0.12}$	$0.93^{+0.32}_{-0.08}$	$0.87^{+0.30}_{-0.07}$	TF	...
HD 110634	HD 110697	$-0.59^{+0.11}_{-0.12}$	$1.22^{+0.05}_{-0.07}$	$0.90^{+0.04}_{-0.05}$	$0.89^{+0.04}_{-0.05}$	TF	T
HD 113556	TYC 8674-2317-1	$-1.55^{+0.46}_{-0.64}$	$1.22^{+0.88}_{-0.53}$	$0.90^{+0.65}_{-0.39}$	$0.99^{+0.71}_{-0.43}$	TF	T
HD 113901	HD 114365	$0.08^{+0.17}_{-0.13}$	$1.24^{+0.12}_{-0.03}$	$0.92^{+0.09}_{-0.02}$	$0.71^{+0.07}_{-0.02}$	TF	...

Table 4 continued

Table 4 (continued)

Star 1	Star 2	t_{ca} (Myr)	d_{ca} (pc)	$d_{ca}/R_{H,T}$	$d_{ca}/R_{H,F}$	Category	IR Excess?
HD 114319	HD 108904	$-0.98^{+0.05}_{-0.05}$	$1.13^{+0.49}_{-0.21}$	$0.81^{+0.35}_{-0.15}$	$0.85^{+0.37}_{-0.16}$	TF	...
HD 115470	HD 115988	$-0.63^{+0.18}_{-0.23}$	$1.57^{+0.30}_{-0.17}$	$0.97^{+0.19}_{-0.11}$	$0.96^{+0.18}_{-0.10}$	TF	...
HD 115600	TYC 8674-2317-1	$0.62^{+0.65}_{-0.26}$	$0.89^{+0.09}_{-0.06}$	$0.65^{+0.07}_{-0.05}$	$0.72^{+0.07}_{-0.05}$	TF	T
HD 116402	HD 114082	$-2.85^{+0.16}_{-0.17}$	$0.87^{+0.36}_{-0.31}$	$0.67^{+0.28}_{-0.24}$	$0.64^{+0.26}_{-0.23}$	TF	TF
HD 119718	HD 116794	$-1.78^{+0.12}_{-0.14}$	$1.27^{+0.39}_{-0.36}$	$0.94^{+0.29}_{-0.27}$	$0.95^{+0.29}_{-0.27}$	TF	T
HD 143215	HD 143844	$-0.44^{+0.07}_{-0.07}$	$1.27^{+0.17}_{-0.16}$	$0.98^{+0.13}_{-0.12}$	$0.97^{+0.12}_{-0.12}$	TF	...
HD 143637	HD 146285	$-2.91^{+0.24}_{-0.29}$	$1.35^{+1.26}_{-0.77}$	$0.98^{+0.92}_{-0.56}$	$0.77^{+0.72}_{-0.44}$	TF	...
HD 144587	HD 144844	$0.23^{+0.35}_{-0.30}$	$1.05^{+1.16}_{-0.26}$	$0.74^{+0.82}_{-0.18}$	$0.65^{+0.71}_{-0.16}$	TF	T
HD 144981	HD 144925	$-0.93^{+0.20}_{-0.27}$	$0.84^{+0.19}_{-0.14}$	$0.54^{+0.12}_{-0.09}$	$0.54^{+0.12}_{-0.09}$	TF	T
HD 144981	HD 145631	$-1.51^{+0.69}_{-1.71}$	$1.27^{+1.99}_{-0.44}$	$0.82^{+1.28}_{-0.28}$	$0.78^{+1.22}_{-0.27}$	TF	TF
HD 145189	HD 144254	$0.76^{+0.17}_{-0.14}$	$1.02^{+0.45}_{-0.28}$	$0.69^{+0.31}_{-0.19}$	$0.66^{+0.29}_{-0.18}$	TF	T
HD 145467	HD 145718	$-2.31^{+0.63}_{-1.03}$	$1.15^{+1.36}_{-0.60}$	$0.80^{+0.94}_{-0.42}$	$0.78^{+0.92}_{-0.41}$	TF	...
HD 146743	HD 147083	$1.42^{+0.83}_{-0.46}$	$1.01^{+0.70}_{-0.34}$	$0.70^{+0.49}_{-0.23}$	$0.69^{+0.48}_{-0.23}$	TF	...
HD 146897	HD 146743	$1.63^{+0.49}_{-0.39}$	$1.12^{+0.53}_{-0.38}$	$0.78^{+0.37}_{-0.26}$	$0.78^{+0.37}_{-0.26}$	TF	T
HD 147220	HD 146416	$0.63^{+0.04}_{-0.04}$	$0.88^{+0.33}_{-0.30}$	$0.62^{+0.23}_{-0.21}$	$0.54^{+0.20}_{-0.18}$	TF	...
HD 150742	HD 150591	$0.38^{+0.33}_{-0.27}$	$1.34^{+0.67}_{-0.32}$	$0.64^{+0.32}_{-0.16}$	$0.71^{+0.35}_{-0.17}$	TF	T
HD 151721	HD 152057	$0.32^{+0.04}_{-0.04}$	$1.16^{+0.14}_{-0.11}$	$0.78^{+0.10}_{-0.07}$	$0.80^{+0.10}_{-0.07}$	TF	T
TYC 8983-854-1	TYC 8983-564-1	$-0.78^{+0.38}_{-0.58}$	$0.69^{+0.53}_{-0.24}$	$0.56^{+0.43}_{-0.20}$	$0.55^{+0.42}_{-0.19}$	TF	...
HD 106797	2MASS J12205449-6457242	$0.07^{+0.18}_{-0.19}$	$1.56^{+0.02}_{-0.03}$	$0.99^{+0.01}_{-0.02}$	$1.29^{+0.01}_{-0.02}$	T	T
HD 106797	CPD-64 1859	$-0.07^{+0.22}_{-0.26}$	$1.52^{+0.19}_{-0.11}$	$0.97^{+0.12}_{-0.09}$	$1.23^{+0.15}_{-0.09}$	T	T
HD 107821	CD-62 657	$0.02^{+0.11}_{-0.11}$	$1.41^{+0.10}_{-0.05}$	$0.95^{+0.06}_{-0.03}$	$1.10^{+0.07}_{-0.04}$	T	...
HD 108483	CD-49 7027	$-1.20^{+1.85}_{-1.44}$	$2.27^{+4.77}_{-1.12}$	$0.96^{+2.02}_{-0.47}$	$1.78^{+3.74}_{-0.88}$	T	...
HD 108501	2MASS J12205449-6457242	$-0.30^{+0.21}_{-0.56}$	$1.55^{+0.29}_{-0.51}$	$0.99^{+0.18}_{-0.33}$	$1.28^{+0.24}_{-0.42}$	T	...
HD 108501	TYC 8983-564-1	$-0.05^{+0.39}_{-0.37}$	$1.55^{+0.44}_{-0.16}$	$0.99^{+0.28}_{-0.10}$	$1.23^{+0.35}_{-0.12}$	T	...
HD 110634	2MASS J12474824-5431308	$-2.17^{+0.36}_{-0.44}$	$1.33^{+0.85}_{-0.61}$	$0.98^{+0.63}_{-0.45}$	$1.23^{+0.79}_{-0.56}$	T	T
HD 120642	CD-51 7721	$1.31^{+0.44}_{-0.27}$	$1.51^{+0.31}_{-0.32}$	$0.85^{+0.18}_{-0.18}$	$1.22^{+0.25}_{-0.26}$	T	...
HD 142315	HD 142097	$0.59^{+0.35}_{-0.22}$	$1.55^{+0.19}_{-0.12}$	$0.95^{+0.12}_{-0.08}$	$1.05^{+0.13}_{-0.08}$	T	T
HD 142315	HD 142705	$-0.20^{+0.62}_{-0.98}$	$1.60^{+0.77}_{-0.77}$	$0.98^{+0.48}_{-0.48}$	$1.03^{+0.50}_{-0.50}$	T	TF
HD 148184	HD 147010	$-0.85^{+0.41}_{-0.49}$	$2.28^{+1.80}_{-1.18}$	$0.98^{+0.77}_{-0.51}$	$1.40^{+1.11}_{-0.73}$	T	...
HD 150742	HD 150287	$0.04^{+0.24}_{-0.24}$	$1.95^{+0.06}_{-0.08}$	$0.94^{+0.03}_{-0.04}$	$1.38^{+0.04}_{-0.06}$	T	T
HD 113524	HD 113703	$1.10^{+0.82}_{-0.52}$	$1.95^{+2.22}_{-0.53}$	$1.47^{+1.67}_{-0.40}$	$0.94^{+1.08}_{-0.26}$	F	T

Table 4 continued

Table 4 (continued)

Star 1	Star 2	t_{ca} (Myr)	d_{ca} (pc)	$d_{\text{ca}}/R_{\text{H,T}}$	$d_{\text{ca}}/R_{\text{H,F}}$	Category	IR Excess?
HD 121835	HD 121190	$-0.13^{+0.26}_{-0.34}$	$1.35^{+0.06}_{-0.22}$	$1.02^{+0.04}_{-0.17}$	$0.83^{+0.04}_{-0.14}$	F	...
HD 137499	HD 137432	$-0.09^{+0.97}_{-0.97}$	$1.62^{+1.06}_{-0.28}$	$1.19^{+0.78}_{-0.21}$	$0.81^{+0.53}_{-0.14}$	F	T
HD 144254	HD 144470	$-0.20^{+0.35}_{-0.43}$	$2.01^{+2.26}_{-1.27}$	$1.29^{+1.45}_{-0.82}$	$0.72^{+0.81}_{-0.46}$	F	...
HD 144587	HD 144175	$0.08^{+1.02}_{-0.87}$	$1.46^{+0.33}_{-0.08}$	$1.03^{+0.23}_{-0.06}$	$0.90^{+0.20}_{-0.05}$	F	T
HD 144587	HD 144661	$0.32^{+0.47}_{-0.59}$	$1.58^{+1.76}_{-0.90}$	$1.11^{+1.24}_{-0.64}$	$0.90^{+1.00}_{-0.51}$	F	T
HD 144844	HD 144661	$0.29^{+0.30}_{-0.28}$	$1.70^{+1.47}_{-0.58}$	$1.04^{+0.90}_{-0.36}$	$0.97^{+0.84}_{-0.33}$	F	...
HD 144925	HD 145502	$0.04^{+0.28}_{-0.30}$	$2.09^{+0.29}_{-0.38}$	$1.34^{+0.18}_{-0.25}$	$0.90^{+0.12}_{-0.17}$	F	...

NOTE—The letters “T” and “F” in the table stand for “target star” and “flyby star”, respectively. In the “Category” column, “T” and “F” denote encounters with $0.5 < d_{\text{ca}}/R_{\text{H,T}} < 1$ and $0.5 < d_{\text{ca}}/R_{\text{H,F}} < 1$, respectively; “TF” denotes encounters satisfying both previous conditions. Those ending with “0.5” denote the fact that $d_{\text{ca}}/R_{\text{H}} \leq 0.5$, where R_{H} is the Hill radius of target star (T), flyby star (F), or both (TF). Similarly, in the “IR Excess” column, “T” or “F” denotes that the target star or the flyby star has IR excess detected, respectively; “TF” denotes that both stars have IR excess detected, according to Cotten & Song 2016.

Table 5. Events identified from USCO sample

Star 1	Star 2	t_{ca} (Myr)	d_{ca} (pc)	$d_{ca}/R_{H,T}$	$d_{ca}/R_{H,F}$	Category	IR Excess?
Gaia DR2 6041813096094711424	Gaia DR2 6041813100399783552	$0.09^{+0.29}_{-0.27}$	$0.16^{+0.41}_{-0.12}$	$0.17^{+0.43}_{-0.12}$	$0.15^{+0.40}_{-0.12}$	TF0.5	...
CD-26 11326	[SMH2016] NV6	$-0.08^{+0.30}_{-0.35}$	$0.54^{+0.31}_{-0.16}$	$0.39^{+0.22}_{-0.12}$	$0.48^{+0.28}_{-0.14}$	TF0.5	...
2MASS J16210010-2536031	2MASS J16211379-2533314	$-0.03^{+0.16}_{-0.16}$	$0.30^{+0.49}_{-0.14}$	$0.24^{+0.39}_{-0.11}$	$0.25^{+0.41}_{-0.12}$	TF0.5	...
HD 146001	2MASS J16145546-2527597	$0.25^{+0.55}_{-0.43}$	$0.46^{+0.80}_{-0.32}$	$0.26^{+0.45}_{-0.32}$	$0.34^{+0.59}_{-0.23}$	TF0.5	...
HD 147196	2MASS J16211450-2342200	$-0.04^{+0.30}_{-0.31}$	$0.43^{+0.77}_{-0.30}$	$0.23^{+0.41}_{-0.16}$	$0.38^{+0.67}_{-0.26}$	TF0.5	...
2MASS J16053815-2039469	2MASS J16035767-2031055	$-0.43^{+0.17}_{-0.39}$	$0.52^{+0.29}_{-0.16}$	$0.49^{+0.27}_{-0.14}$	$0.43^{+0.24}_{-0.13}$	TF0.5	...
UCAC4 354-076591	2MASS J16111742-1918285	$0.19^{+1.11}_{-0.98}$	$0.47^{+0.25}_{-0.10}$	$0.44^{+0.24}_{-0.09}$	$0.45^{+0.24}_{-0.10}$	TF0.5	...
UCAC4 354-076591	Wa Oph 2	$-0.05^{+0.15}_{-0.14}$	$0.46^{+0.50}_{-0.18}$	$0.43^{+0.47}_{-0.17}$	$0.36^{+0.39}_{-0.14}$	TF0.5	...
2MASS J16053153-1945435	ScOPMS 28	$0.11^{+0.27}_{-0.23}$	$0.32^{+0.62}_{-0.07}$	$0.29^{+0.58}_{-0.07}$	$0.32^{+0.64}_{-0.07}$	TF0.5	...
2MASS J16051687-1948374	ScOPMS 28	$-0.12^{+0.26}_{-0.22}$	$0.36^{+0.77}_{-0.22}$	$0.32^{+0.68}_{-0.19}$	$0.37^{+0.80}_{-0.23}$	TF0.5	...
ASAS J160811-1904.9	HD 144925	$-0.35^{+0.20}_{-0.25}$	$0.37^{+0.27}_{-0.10}$	$0.29^{+0.21}_{-0.08}$	$0.24^{+0.17}_{-0.07}$	TF0.5	...
b Sco	CD-25 11133	$0.23^{+1.25}_{-1.39}$	$1.10^{+3.15}_{-0.81}$	$0.42^{+1.20}_{-0.31}$	$0.80^{+2.27}_{-0.58}$	T0.5	...
b Sco	HD 141618	$-0.01^{+1.73}_{-1.72}$	$0.95^{+2.80}_{-0.51}$	$0.36^{+1.07}_{-0.19}$	$0.69^{+2.05}_{-0.37}$	T0.5	...
CD-23 12602	UCAC4 334-078461	$-0.16^{+0.56}_{-0.64}$	$0.60^{+0.31}_{-0.14}$	$0.44^{+0.23}_{-0.10}$	$0.54^{+0.27}_{-0.12}$	T0.5	T
HD 142705	UCAC4 336-078484	$-0.01^{+0.58}_{-0.64}$	$0.52^{+0.17}_{-0.09}$	$0.34^{+0.11}_{-0.06}$	$0.51^{+0.17}_{-0.08}$	T0.5	T
HD 146366	2MASS J16172297-2121119	$-0.03^{+0.05}_{-0.05}$	$0.66^{+0.10}_{-0.08}$	$0.48^{+0.07}_{-0.06}$	$0.68^{+0.10}_{-0.08}$	T0.5	...
ω Sco	2MASS J16053815-2039469	$-0.29^{+0.54}_{-0.74}$	$1.21^{+1.38}_{-0.51}$	$0.44^{+0.50}_{-0.18}$	$1.13^{+1.29}_{-0.48}$	T0.5	...
ν Sco A	UCAC4 354-076591	$0.12^{+0.54}_{-0.56}$	$1.15^{+0.78}_{-0.66}$	$0.49^{+0.34}_{-0.28}$	$1.07^{+0.73}_{-0.61}$	T0.5	...
HD 144925	2MASS J16064794-1841437	$-1.32^{+0.26}_{-0.40}$	$0.73^{+0.28}_{-0.24}$	$0.47^{+0.18}_{-0.15}$	$0.68^{+0.27}_{-0.22}$	T0.5	...
HD 144586	2MASS J16083138-1802414	$-1.01^{+0.34}_{-0.34}$	$0.73^{+0.20}_{-0.16}$	$0.45^{+0.12}_{-0.10}$	$0.68^{+0.19}_{-0.15}$	T0.5	T
Gaia DR2 6045624866694553856	HD 147648	$-0.29^{+0.03}_{-0.03}$	$0.80^{+0.21}_{-0.12}$	$0.67^{+0.18}_{-0.10}$	$0.45^{+0.12}_{-0.07}$	F0.5	...
EPIC 203390805	HD 147648	$-0.32^{+0.04}_{-0.04}$	$0.60^{+0.15}_{-0.10}$	$0.56^{+0.14}_{-0.09}$	$0.34^{+0.08}_{-0.05}$	F0.5	...
ROXs 12	HD 147701	$-0.29^{+0.18}_{-0.31}$	$0.92^{+1.03}_{-0.54}$	$0.86^{+0.96}_{-0.51}$	$0.46^{+0.52}_{-0.27}$	F0.5	...
EPIC 204184435	HD 145333	$-0.20^{+0.16}_{-0.19}$	$0.65^{+0.35}_{-0.29}$	$0.51^{+0.27}_{-0.23}$	$0.45^{+0.24}_{-0.20}$	F0.5	...
[PGZ2001] J161031.9-191305	HD 144925	$0.25^{+0.48}_{-0.35}$	$0.75^{+0.91}_{-0.33}$	$0.65^{+0.80}_{-0.29}$	$0.48^{+0.59}_{-0.21}$	F0.5	...
TYC 6804-148-1	HD 149598	$-0.18^{+0.30}_{-0.30}$	$0.95^{+1.15}_{-0.52}$	$0.69^{+0.83}_{-0.38}$	$0.70^{+0.84}_{-0.38}$	TF	...
2MASS J16332693-2616274	DoAr 61	$0.43^{+1.26}_{-1.88}$	$0.85^{+0.23}_{-0.14}$	$0.75^{+0.20}_{-0.13}$	$0.69^{+0.19}_{-0.12}$	TF	...
HD 147255	2MASS J16161720-2609101	$-0.62^{+0.08}_{-0.09}$	$1.06^{+0.22}_{-0.20}$	$0.77^{+0.16}_{-0.15}$	$0.86^{+0.18}_{-0.17}$	TF	...
2MASS J16161720-2609101	HD 146331	$0.15^{+0.87}_{-0.74}$	$1.03^{+1.25}_{-0.63}$	$0.83^{+1.01}_{-0.51}$	$0.63^{+0.77}_{-0.39}$	TF	...

Table 5 continued

Table 5 (continued)

Star 1	Star 2	t_{ca} (Myr)	d_{ca} (pc)	$d_{\text{ca}}/R_{\text{H},\text{T}}$	$d_{\text{ca}}/R_{\text{H},\text{F}}$	Category	IR Excess?
2MASS J16212918-2405190	HD 147196	$-0.02^{+0.18}_{-0.13}$	$1.06^{+0.57}_{-0.13}$	$0.90^{+0.48}_{-0.17}$	$0.57^{+0.31}_{-0.07}$	TF	...
Gaia DR2 6050024970485018624	Gaia DR2 6050047785351251712	$-0.05^{+1.37}_{-1.13}$	$0.99^{+0.52}_{-0.36}$	$0.84^{+0.44}_{-0.30}$	$0.84^{+0.44}_{-0.30}$	TF	...
Gaia DR2 6050047785351251712	CD-23 12840A	$-0.01^{+0.33}_{-0.29}$	$1.04^{+1.15}_{-0.50}$	$0.88^{+0.98}_{-0.43}$	$0.77^{+0.86}_{-0.37}$	TF	...
RX J1620.7-2348	HD 147196	$-0.27^{+1.55}_{-0.94}$	$0.95^{+1.51}_{-0.67}$	$0.76^{+1.21}_{-0.54}$	$0.51^{+0.81}_{-0.36}$	TF	...
2MASS J16151239-2318453	2MASS J16132929-2311075	$-0.29^{+0.58}_{-0.57}$	$1.05^{+0.44}_{-0.05}$	$0.89^{+0.38}_{-0.05}$	$0.81^{+0.34}_{-0.04}$	TF	...
HD 142933	UCAC4 334-078461	$-2.16^{+0.48}_{-0.71}$	$0.99^{+0.80}_{-0.42}$	$0.72^{+0.58}_{-0.31}$	$0.89^{+0.72}_{-0.38}$	TF	...
RX J1602.8-2401B	EPIC 204063024	$-0.11^{+0.73}_{-0.58}$	$0.70^{+0.13}_{-0.11}$	$0.56^{+0.11}_{-0.11}$	$0.77^{+0.15}_{-0.15}$	TF	...
CD-25 11133	HD 141618	$0.39^{+0.94}_{-1.17}$	$0.97^{+1.91}_{-0.71}$	$0.70^{+1.38}_{-0.32}$	$0.71^{+1.40}_{-0.52}$	TF	...
UCAC4 334-078461	HD 142249	$-2.85^{+0.77}_{-1.45}$	$0.85^{+1.34}_{-0.47}$	$0.76^{+1.20}_{-0.42}$	$0.61^{+0.97}_{-0.34}$	TF	...
UCAC4 334-078461	UCAC4 336-078484	$0.06^{+0.73}_{-0.67}$	$0.99^{+0.35}_{-0.10}$	$0.89^{+0.32}_{-0.09}$	$0.96^{+0.34}_{-0.10}$	TF	...
HD 142705	CD-23 12602	$0.25^{+1.12}_{-0.74}$	$1.07^{+0.53}_{-0.30}$	$0.69^{+0.34}_{-0.19}$	$0.79^{+0.39}_{-0.22}$	TF	TF
HD 142705	UCAC4 334-078461	$-0.03^{+1.06}_{-0.86}$	$0.87^{+0.71}_{-0.41}$	$0.56^{+0.46}_{-0.26}$	$0.78^{+0.64}_{-0.37}$	TF	T
2MASS J16110479-2333166	UCAC4 333-083075	$-0.48^{+2.27}_{-1.48}$	$0.73^{+0.72}_{-0.18}$	$0.68^{+0.67}_{-0.17}$	$0.68^{+0.67}_{-0.17}$	TF	...
2MASS J16110479-2333166	HD 145333	$0.01^{+0.20}_{-0.15}$	$0.97^{+0.23}_{-0.09}$	$0.90^{+0.22}_{-0.08}$	$0.67^{+0.16}_{-0.06}$	TF	...
Gaia DR2 6242198746659039872	2MASS J16120920-2247504	$0.27^{+0.76}_{-1.31}$	$0.90^{+0.87}_{-0.33}$	$0.93^{+0.90}_{-0.34}$	$0.84^{+0.81}_{-0.30}$	TF	...
2MASS J16125889-2245202	HD 145718	$0.15^{+0.69}_{-0.83}$	$0.93^{+0.96}_{-0.18}$	$0.87^{+0.90}_{-0.17}$	$0.65^{+0.68}_{-0.13}$	TF	...
2MASS J16120920-2247504	HD 145718	$-1.96^{+0.63}_{-1.25}$	$1.04^{+0.63}_{-0.33}$	$0.97^{+0.59}_{-0.31}$	$0.73^{+0.44}_{-0.23}$	TF	...
2MASS J16120920-2247504	BD-21 4301	$-0.71^{+0.32}_{-0.70}$	$0.97^{+1.13}_{-0.26}$	$0.91^{+1.06}_{-0.24}$	$0.74^{+0.86}_{-0.20}$	TF	...
HD 145468	BD-21 4301	$-0.21^{+0.15}_{-0.22}$	$1.04^{+0.07}_{-0.16}$	$0.70^{+0.05}_{-0.11}$	$0.79^{+0.05}_{-0.12}$	TF	...
HD 145718	BD-21 4301	$-1.20^{+0.36}_{-0.73}$	$1.30^{+1.54}_{-0.79}$	$0.92^{+1.08}_{-0.55}$	$0.99^{+1.17}_{-0.60}$	TF	...
HD 145718	HD 145467	$-2.31^{+0.63}_{-1.03}$	$1.16^{+1.36}_{-0.60}$	$0.81^{+0.95}_{-0.42}$	$0.80^{+0.94}_{-0.42}$	TF	...
EPIC 204554162	HD 146366	$0.59^{+0.07}_{-0.07}$	$0.77^{+0.29}_{-0.24}$	$0.72^{+0.27}_{-0.23}$	$0.56^{+0.21}_{-0.18}$	TF	...
HD 146366	HD 146743	$0.09^{+0.05}_{-0.05}$	$1.00^{+0.03}_{-0.01}$	$0.73^{+0.02}_{-0.01}$	$0.73^{+0.02}_{-0.01}$	TF	...
CD-22 11315	HD 143600	$-0.36^{+1.13}_{-1.11}$	$0.82^{+1.14}_{-0.25}$	$0.62^{+0.86}_{-0.19}$	$0.51^{+0.71}_{-0.16}$	TF	...
2MASS J16022461-2200248	EPIC 204548337	$-0.07^{+0.31}_{-0.31}$	$0.85^{+0.48}_{-0.19}$	$0.82^{+0.47}_{-0.18}$	$0.87^{+0.50}_{-0.19}$	TF	...
HD 143567	TYC 6212-1023-1	$-0.13^{+0.71}_{-0.85}$	$0.88^{+0.17}_{-0.09}$	$0.54^{+0.11}_{-0.06}$	$0.74^{+0.15}_{-0.08}$	TF	...
2MASS J16085673-2033460	IRXS J160801.7-202755	$-0.06^{+0.34}_{-0.36}$	$0.81^{+0.94}_{-0.41}$	$0.67^{+0.78}_{-0.34}$	$0.76^{+0.88}_{-0.39}$	TF	...
2MASS J16053815-2039469	2MASS J16053153-1945435	$-0.80^{+0.27}_{-0.52}$	$0.69^{+0.63}_{-0.37}$	$0.64^{+0.59}_{-0.37}$	$0.64^{+0.59}_{-0.37}$	TF	...
RX J1603.9-2031B	2MASS J16035767-2031055	$0.96^{+1.80}_{-1.23}$	$0.71^{+2.06}_{-0.48}$	$0.66^{+1.92}_{-0.45}$	$0.58^{+1.69}_{-0.40}$	TF	...
HD 145554	UCAC4 354-076591	$0.01^{+0.70}_{-0.43}$	$0.85^{+0.51}_{-0.31}$	$0.52^{+0.31}_{-0.19}$	$0.80^{+0.47}_{-0.29}$	TF	T
HD 145554	2MASS J16111742-1918285	$0.01^{+0.59}_{-0.42}$	$0.92^{+0.41}_{-0.25}$	$0.57^{+0.25}_{-0.15}$	$0.87^{+0.39}_{-0.24}$	TF	T

Table 5 continued

Table 5 (continued)

Star 1	Star 2	t_{ca} (Myr)	d_{ca} (pc)	$d_{ca}/R_{H,T}$	$d_{ca}/R_{H,F}$	Category	IR Excess?
HD 145554	Wa Oph 2	$-0.07^{+0.26}_{-0.27}$	$1.20^{+0.51}_{-0.19}$	$0.74^{+0.31}_{-0.12}$	$0.92^{+0.39}_{-0.15}$	TF	T
UCAC4 354-076591	BD-18 4244	$-0.34^{+0.53}_{-0.33}$	$0.98^{+1.48}_{-0.71}$	$0.91^{+1.38}_{-0.66}$	$0.82^{+1.24}_{-0.60}$	TF	...
2MASS J16111742-1918285	[PGZ2001] J161031.9-191305	$-0.22^{+0.86}_{-0.61}$	$0.70^{+1.20}_{-0.25}$	$0.66^{+1.14}_{-0.23}$	$0.61^{+1.05}_{-0.23}$	TF	...
2MASS J16111742-1918285	Wa Oph 2	$0.02^{+0.17}_{-0.18}$	$0.71^{+0.47}_{-0.11}$	$0.67^{+0.45}_{-0.11}$	$0.55^{+0.37}_{-0.09}$	TF	...
2MASS J16111742-1918285	BD-18 4244	$-0.34^{+0.34}_{-0.37}$	$0.91^{+1.17}_{-0.27}$	$0.86^{+1.11}_{-0.26}$	$0.77^{+0.99}_{-0.23}$	TF	...
HD 143956	2MASS J16051687-1948374	$0.12^{+0.44}_{-0.43}$	$0.89^{+0.48}_{-0.14}$	$0.55^{+0.30}_{-0.08}$	$0.78^{+0.42}_{-0.12}$	TF	T
HD 143956	ScoPMS 28	$-0.09^{+0.15}_{-0.21}$	$0.96^{+0.04}_{-0.02}$	$0.59^{+0.02}_{-0.01}$	$0.99^{+0.04}_{-0.02}$	TF	T
2MASS J16052157-1821412	2MASS J16052076-1821367	$0.16^{+0.36}_{-0.49}$	$0.76^{+1.44}_{-0.54}$	$0.61^{+1.16}_{-0.43}$	$0.85^{+1.60}_{-0.60}$	TF	...
HD 144586	ASAS J160811-1904.9	$-1.64^{+0.65}_{-1.29}$	$1.19^{+0.97}_{-0.64}$	$0.73^{+0.60}_{-0.39}$	$0.94^{+0.76}_{-0.50}$	TF	T
χ Oph	2MASS J16171596-1947041	$-1.68^{+0.52}_{-0.67}$	$2.28^{+2.05}_{-1.04}$	$0.98^{+0.88}_{-0.45}$	$1.92^{+1.73}_{-0.88}$	T	...
HD 146001	2MASS J16130234-2501460	$0.47^{+1.31}_{-1.27}$	$1.65^{+1.12}_{-0.29}$	$0.94^{+0.64}_{-0.16}$	$1.84^{+1.25}_{-0.32}$	T	...
HD 146285	2MASS J16173031-2438390	$-0.02^{+0.09}_{-0.10}$	$1.14^{+0.05}_{-0.10}$	$0.65^{+0.03}_{-0.06}$	$1.07^{+0.05}_{-0.09}$	T	...
HD 147196	2MASS J16212844-2312110	$0.05^{+0.24}_{-0.20}$	$1.24^{+0.19}_{-0.07}$	$0.66^{+0.10}_{-0.04}$	$1.08^{+0.17}_{-0.06}$	T	...
HD 146706	EPIC 204184435	$1.59^{+0.90}_{-0.60}$	$1.31^{+3.00}_{-0.69}$	$0.81^{+1.85}_{-0.42}$	$1.03^{+2.36}_{-0.54}$	T	...
HD 146367	2MASS J16151239-2318453	$-0.97^{+0.28}_{-0.61}$	$1.27^{+0.32}_{-0.18}$	$0.89^{+0.22}_{-0.13}$	$1.07^{+0.27}_{-0.15}$	T	...
HD 143472	2MASS J16001330-2418106	$-0.99^{+0.43}_{-0.82}$	$1.26^{+3.67}_{-0.57}$	$0.85^{+2.46}_{-0.38}$	$1.22^{+3.54}_{-0.55}$	T	...
HD 142705	UCAC4 337-077055	$-0.14^{+0.67}_{-1.22}$	$1.40^{+0.44}_{-0.40}$	$0.90^{+0.29}_{-0.26}$	$1.50^{+0.49}_{-0.45}$	T	T
UCAC4 336-078484	UCAC4 337-077055	$-0.02^{+0.45}_{-0.70}$	$0.93^{+0.27}_{-0.18}$	$0.89^{+0.26}_{-0.17}$	$1.03^{+0.30}_{-0.20}$	T	...
HD 142315	UCAC4 336-078484	$-0.17^{+0.46}_{-0.79}$	$1.36^{+0.50}_{-0.45}$	$0.83^{+0.30}_{-0.28}$	$1.31^{+0.48}_{-0.43}$	T	T
HD 144661	HD 144844	$0.29^{+0.30}_{-0.28}$	$1.70^{+1.47}_{-0.58}$	$0.97^{+0.84}_{-0.33}$	$1.04^{+0.90}_{-0.36}$	T	...
HD 144822	2MASS J16053815-2039469	$0.56^{+0.30}_{-0.18}$	$1.41^{+0.14}_{-0.13}$	$0.98^{+0.10}_{-0.09}$	$1.32^{+0.12}_{-0.12}$	T	...
ω Sco	IRXS J160801.7-202755	$0.16^{+0.98}_{-1.08}$	$2.32^{+4.07}_{-1.62}$	$0.84^{+1.47}_{-0.58}$	$2.17^{+3.80}_{-1.51}$	T	...
HD 145554	[PGZ2001] J161031.9-191305	$0.03^{+0.71}_{-0.78}$	$1.38^{+0.41}_{-0.07}$	$0.84^{+0.25}_{-0.04}$	$1.20^{+0.36}_{-0.06}$	T	T
HD 145554	BD-18 4244	$-0.18^{+0.48}_{-0.64}$	$1.43^{+0.97}_{-0.65}$	$0.88^{+0.59}_{-0.40}$	$1.21^{+0.82}_{-0.55}$	T	T
HD 145631	2MASS J16093909-1955023	$-0.78^{+0.37}_{-0.84}$	$1.45^{+0.40}_{-0.48}$	$0.89^{+0.25}_{-0.30}$	$1.30^{+0.36}_{-0.43}$	T	T
HD 145631	UCAC4 354-076591	$0.45^{+0.51}_{-1.16}$	$1.62^{+1.29}_{-0.63}$	$1.00^{+0.79}_{-0.39}$	$1.52^{+1.21}_{-0.59}$	T	T
ν Sco A	2MASS J16111742-1918285	$0.10^{+0.62}_{-0.63}$	$1.38^{+1.02}_{-0.88}$	$0.59^{+0.44}_{-0.38}$	$1.30^{+0.96}_{-0.83}$	T	...
ν Sco A	[PGZ2001] J161031.9-191305	$-0.16^{+0.42}_{-0.48}$	$1.40^{+2.24}_{-0.71}$	$0.60^{+0.96}_{-0.31}$	$1.22^{+1.96}_{-0.62}$	T	...
ν Sco A	Wa Oph 2	$0.06^{+0.38}_{-0.39}$	$1.71^{+1.53}_{-0.94}$	$0.74^{+0.66}_{-0.41}$	$1.32^{+1.18}_{-0.73}$	T	...
ν Sco A	BD-18 4244	$-0.08^{+0.43}_{-0.44}$	$1.65^{+1.34}_{-0.87}$	$0.71^{+0.58}_{-0.37}$	$1.39^{+1.13}_{-0.73}$	T	...
ν Sco A	HD 144925	$0.04^{+0.28}_{-0.30}$	$2.09^{+0.29}_{-0.38}$	$0.90^{+0.12}_{-0.16}$	$1.34^{+0.18}_{-0.25}$	T	...

Table 5 continued

Table 5 (continued)

Star 1	Star 2	t_{ca} (Myr)	d_{ca} (pc)	$d_{\text{ca}}/R_{\text{H},\text{T}}$	$d_{\text{ca}}/R_{\text{H},\text{F}}$	Category	IR Excess?
HD 144981	2MASS J16093909-1955023	$0.80^{+3.17}_{-4.07}$	$1.44^{+1.84}_{-0.47}$	$0.93^{+1.19}_{-0.30}$	$1.29^{+1.65}_{-0.42}$	T	T
HD 144981	ASAS J160811-1904.9	$-2.02^{+1.28}_{-2.80}$	$1.48^{+2.14}_{-0.66}$	$0.95^{+1.38}_{-0.42}$	$1.16^{+1.69}_{-0.52}$	T	T
Wa Oph 2	BD-18 4244	$0.03^{+0.28}_{-0.40}$	$1.26^{+1.11}_{-0.74}$	$0.97^{+0.85}_{-0.37}$	$1.06^{+0.93}_{-0.62}$	T	...
HD 143956	2MASS J16053815-2039469	$-0.92^{+0.25}_{-0.46}$	$1.46^{+0.28}_{-0.45}$	$0.90^{+0.17}_{-0.28}$	$1.36^{+0.26}_{-0.42}$	T	T
HD 144569	ScOPMS 45	$-1.37^{+0.37}_{-0.55}$	$1.46^{+0.63}_{-0.64}$	$0.91^{+0.39}_{-0.40}$	$1.20^{+0.52}_{-0.53}$	T	T
[SMH2016] NV6	HD 147592	$0.02^{+0.47}_{-0.45}$	$1.52^{+0.09}_{-0.03}$	$1.36^{+0.08}_{-0.03}$	$0.98^{+0.06}_{-0.02}$	F	...
2MASS J16153587-2529008	HD 146285	$0.07^{+0.11}_{-0.10}$	$1.38^{+0.12}_{-0.08}$	$1.13^{+0.10}_{-0.07}$	$0.78^{+0.07}_{-0.05}$	F	...
ROXs 12	EPIC 203725441	$0.05^{+0.12}_{-0.24}$	$1.34^{+0.56}_{-0.45}$	$1.25^{+0.52}_{-0.42}$	$0.98^{+0.41}_{-0.33}$	F	...
EPIC 203725441	HD 147701	$-0.30^{+1.93}_{-1.28}$	$1.64^{+1.64}_{-0.72}$	$1.20^{+1.20}_{-0.53}$	$0.82^{+0.82}_{-0.36}$	F	...
Gaia DR2 6049726075120913152	HD 145792A	$-1.29^{+0.56}_{-0.96}$	$1.44^{+0.73}_{-0.37}$	$1.22^{+0.61}_{-0.31}$	$0.76^{+0.38}_{-0.19}$	F	...
EPIC 203893268	HD 144844	$0.55^{+0.62}_{-0.32}$	$1.31^{+0.85}_{-0.67}$	$1.22^{+0.80}_{-0.62}$	$0.80^{+0.52}_{-0.41}$	F	...
2MASS J16212844-2312110	HD 146706	$-0.40^{+0.28}_{-0.51}$	$1.24^{+1.17}_{-0.35}$	$1.08^{+1.03}_{-0.31}$	$0.76^{+0.72}_{-0.22}$	F	...
EPIC 204063024	HD 144175	$-0.19^{+0.45}_{-0.68}$	$1.01^{+0.62}_{-0.35}$	$1.12^{+0.69}_{-0.39}$	$0.62^{+0.38}_{-0.21}$	F	...
2MASS J16110479-2333166	EPIC 204184435	$-0.02^{+0.23}_{-0.21}$	$1.26^{+0.13}_{-0.02}$	$1.18^{+0.12}_{-0.02}$	$0.99^{+0.10}_{-0.01}$	F	...
EPIC 204184435	BD-21 4301	$-1.77^{+0.70}_{-1.70}$	$1.32^{+4.24}_{-0.69}$	$1.04^{+3.34}_{-0.54}$	$1.00^{+3.22}_{-0.52}$	F	...
Gaia DR2 6242198746659039872	HD 145718	$-1.03^{+0.48}_{-1.26}$	$1.12^{+0.38}_{-0.48}$	$1.15^{+0.39}_{-0.49}$	$0.79^{+0.27}_{-0.34}$	F	...
Gaia DR2 6242198746659039872	BD-21 4301	$-0.95^{+0.56}_{-1.07}$	$1.29^{+4.94}_{-0.71}$	$1.33^{+5.09}_{-0.74}$	$0.98^{+3.75}_{-0.54}$	F	...
2MASS J16022461-2200248	2MASS J16004056-2200322	$0.05^{+0.32}_{-0.33}$	$1.16^{+0.38}_{-0.13}$	$1.12^{+0.36}_{-0.12}$	$0.94^{+0.30}_{-0.10}$	F	...
EPIC 204548337	2MASS J16042165-2130284	$0.33^{+0.56}_{-0.59}$	$1.06^{+1.03}_{-0.69}$	$1.09^{+1.06}_{-0.71}$	$0.82^{+0.79}_{-0.53}$	F	...
V1150 Sco	HD 143567	$-0.09^{+0.71}_{-0.54}$	$1.46^{+0.48}_{-0.09}$	$1.50^{+0.49}_{-0.10}$	$0.89^{+0.29}_{-0.06}$	F	...
EPIC 204787127	ω Sco	$-0.05^{+0.90}_{-1.12}$	$2.41^{+3.81}_{-1.56}$	$2.68^{+4.24}_{-1.74}$	$0.87^{+1.37}_{-0.56}$	F	...
2MASS J16111742-1918285	HD 144925	$-0.01^{+0.14}_{-0.14}$	$1.48^{+0.09}_{-0.10}$	$1.40^{+0.08}_{-0.09}$	$0.95^{+0.06}_{-0.06}$	F	...

NOTE—The notations in this table are the same as in Table 4. The target and flyby stars are presented using the *Gaia* DR2 identifiers. Only Gaia DR2 6237422850406493952 (HD 142315) has been observed by Esposito et al. (2020) but no disk was detected.

Table 6. Events involving candidates and field stars with $d_{\text{ca}} < 1$ pc and $v_{\text{rel}} < 10 \text{ km s}^{-1}$

Star 1	Star 2	t_{ca} (Myr)	d_{ca} (pc)	v_{rel} (km s^{-1})	Category
Gaia DR2 3463980463840622848	Gaia DR2 3463980459544094208	$0.01^{+0.33}_{-0.34}$	$0.39^{+0.46}_{-0.28}$	$0.80^{+0.24}_{-0.10}$	F
Gaia DR2 3481965141177021568	Gaia DR2 3481965995873045888	$-0.19^{+0.53}_{-0.36}$	$0.25^{+0.59}_{-0.18}$	$4.80^{+4.83}_{-3.15}$	F
Gaia DR2 4126469681670065408	Gaia DR2 4126469685970383360	$-0.53^{+0.27}_{-0.31}$	$0.42^{+0.25}_{-0.20}$	$3.96^{+0.83}_{-0.82}$	C
Gaia DR2 5334680613863027200	Gaia DR2 5334681571583520512	$-0.43^{+0.51}_{-0.63}$	$0.61^{+0.89}_{-0.32}$	$7.66^{+2.29}_{-2.28}$	C
Gaia DR2 5341470132513014272	Gaia DR2 5341856262911551872	$0.29^{+0.57}_{-1.36}$	$0.81^{+0.28}_{-0.31}$	$1.91^{+1.98}_{-1.25}$	C
Gaia DR2 5343524947923387520	Gaia DR2 5342085785963213184	$-1.10^{+0.37}_{-0.75}$	$0.97^{+0.30}_{-0.30}$	$5.93^{+2.33}_{-2.33}$	C
Gaia DR2 5343610331876174336	Gaia DR2 5343603288120259072	$-0.18^{+0.32}_{-0.26}$	$0.79^{+0.92}_{-0.22}$	$4.39^{+3.71}_{-1.90}$	C
Gaia DR2 5359955053246566144	Gaia DR2 5347989239999386240	$0.41^{+0.23}_{-0.12}$	$0.76^{+0.08}_{-0.04}$	$3.08^{+1.16}_{-1.15}$	F
Gaia DR2 5855799303791243776	Gaia DR2 5855802430512817152	$0.08^{+0.06}_{-0.05}$	$0.31^{+0.02}_{-0.01}$	$9.04^{+2.64}_{-2.64}$	C
Gaia DR2 5855799303791243776	Gaia DR2 5855802808484620288	$0.09^{+0.07}_{-0.05}$	$0.21^{+0.02}_{-0.02}$	$8.27^{+2.60}_{-2.60}$	C
Gaia DR2 5862028930545927936	Gaia DR2 5862081981988722048	$-0.53^{+1.79}_{-1.09}$	$0.79^{+1.59}_{-0.39}$	$5.66^{+5.97}_{-3.81}$	C
Gaia DR2 5907308051965769216	Gaia DR2 5907311870203075456	$0.03^{+0.33}_{-0.39}$	$0.41^{+0.62}_{-0.23}$	$5.27^{+5.46}_{-3.34}$	C
Gaia DR2 5964856323071807360	Gaia DR2 5967459073270375936	$-2.43^{+0.53}_{-0.83}$	$0.81^{+0.50}_{-0.36}$	$5.41^{+1.33}_{-1.32}$	C
Gaia DR2 5969081333984323584	Gaia DR2 5969095215321931008	$0.33^{+0.69}_{-0.54}$	$0.63^{+0.21}_{-0.06}$	$3.38^{+1.45}_{-1.42}$	C
Gaia DR2 5997082081177906048	Gaia DR2 5997022192152593664	$1.78^{+1.65}_{-0.78}$	$0.81^{+1.59}_{-0.33}$	$3.88^{+2.13}_{-2.03}$	C
Gaia DR2 5997082081177906048	Gaia DR2 5997034252420531712	$0.37^{+0.38}_{-0.32}$	$0.50^{+0.47}_{-0.23}$	$8.27^{+2.31}_{-2.27}$	C
Gaia DR2 5997082081177906048	Gaia DR2 5997035317572422912	$0.31^{+1.09}_{-0.94}$	$0.40^{+1.14}_{-0.26}$	$5.29^{+2.51}_{-2.44}$	C
Gaia DR2 5997082081177906048	Gaia DR2 5997081909379214080	$-0.05^{+0.23}_{-0.24}$	$0.30^{+0.40}_{-0.22}$	$9.87^{+2.60}_{-2.57}$	F
Gaia DR2 5997082081177906048	Gaia DR2 5997082046818384768	$0.38^{+1.25}_{-1.03}$	$0.30^{+0.85}_{-0.22}$	$3.15^{+2.22}_{-1.92}$	C
Gaia DR2 5997082081177906048	Gaia DR2 5997082390415552768	$0.34^{+0.65}_{-0.48}$	$0.23^{+0.35}_{-0.10}$	$4.35^{+2.33}_{-2.27}$	C
Gaia DR2 5997082081177906048	Gaia DR2 5997082768372892160	$0.35^{+0.81}_{-0.59}$	$0.15^{+0.39}_{-0.07}$	$4.92^{+3.11}_{-2.91}$	C
Gaia DR2 5997082081177906048	Gaia DR2 5997082871452217344	$0.72^{+0.97}_{-0.60}$	$0.28^{+0.42}_{-0.14}$	$4.14^{+2.23}_{-2.16}$	C
Gaia DR2 5997082081177906048	Gaia DR2 5997409254599602688	$0.59^{+0.57}_{-0.46}$	$0.78^{+0.21}_{-0.12}$	$6.89^{+2.04}_{-2.04}$	C
Gaia DR2 5997082081177906048	Gaia DR2 5997410491550194816	$-0.17^{+0.39}_{-0.42}$	$0.44^{+0.59}_{-0.25}$	$5.82^{+2.41}_{-2.37}$	C
Gaia DR2 5997082081177906048	Gaia DR2 5997457736191421184	$-0.25^{+0.33}_{-0.37}$	$0.61^{+0.61}_{-0.35}$	$7.93^{+2.42}_{-2.40}$	F
Gaia DR2 5997082081177906048	Gaia DR2 5997457736191421440	$0.11^{+0.33}_{-0.32}$	$0.28^{+0.39}_{-0.19}$	$8.05^{+1.74}_{-1.73}$	C
Gaia DR2 5997082081177906048	Gaia DR2 5997490206145065088	$1.38^{+1.11}_{-0.68}$	$0.92^{+1.41}_{-0.29}$	$3.32^{+1.87}_{-1.57}$	C
Gaia DR2 5997082115537645696	Gaia DR2 5997410491550194816	$-0.07^{+0.31}_{-0.29}$	$0.99^{+1.20}_{-0.64}$	$6.81^{+2.15}_{-1.89}$	C
Gaia DR2 5997082115537645696	Gaia DR2 5997457736191421440	$0.13^{+0.31}_{-0.28}$	$0.88^{+0.94}_{-0.60}$	$8.89^{+1.58}_{-1.52}$	C

Table 6 continued

Table 6 (continued)

Star 1	Star 2	t_{ca} (Myr)	d_{ca} (pc)	v_{rel} (km s $^{-1}$)	Category
Gaia DR2 5997809579916196608	Gaia DR2 5997809579916196480	0.05 $^{+0.26}_{-0.30}$	0.83 $^{+1.30}_{-0.60}$	6.68 $^{+5.99}_{-3.06}$	C
Gaia DR2 6002639803206476672	Gaia DR2 6002610666147516544	-0.04 $^{+0.27}_{-0.45}$	0.65 $^{+0.37}_{-0.25}$	3.13 $^{+2.98}_{-1.77}$	C
Gaia DR2 6007264520906861824	Gaia DR2 6007264516610101376	-0.20 $^{+0.76}_{-0.82}$	0.33 $^{+1.30}_{-0.28}$	7.57 $^{+6.68}_{-5.04}$	C
Gaia DR2 6009052258106701312	Gaia DR2 6009033291530588928	-0.49 $^{+0.24}_{-0.45}$	0.52 $^{+0.80}_{-0.22}$	8.30 $^{+4.35}_{-4.19}$	C
Gaia DR2 6010721900869155584	Gaia DR2 6010721900869155328	0.07 $^{+0.23}_{-0.23}$	0.16 $^{+0.23}_{-0.11}$	2.52 $^{+1.02}_{-0.96}$	F
Gaia DR2 6013074512147971072	Gaia DR2 6013065853493820416	0.10 $^{+2.01}_{-2.28}$	0.68 $^{+0.48}_{-0.34}$	0.71 $^{+0.64}_{-0.36}$	C
Gaia DR2 6013398451460692992	Gaia DR2 6013399830146943104	0.20 $^{+0.51}_{-0.42}$	0.45 $^{+0.49}_{-0.16}$	4.93 $^{+2.15}_{-2.06}$	C
Gaia DR2 6013398451460692992	Gaia DR2 6013399894569703040	-0.09 $^{+0.15}_{-0.16}$	0.37 $^{+0.24}_{-0.14}$	9.98 $^{+2.35}_{-2.32}$	C
Gaia DR2 6021142934659068288	Gaia DR2 6021156025719468800	-0.02 $^{+0.32}_{-0.29}$	0.66 $^{+0.80}_{-0.37}$	5.43 $^{+2.80}_{-2.33}$	C
Gaia DR2 6042459132190170496	Gaia DR2 6042459132197205504	0.00 $^{+0.16}_{-0.16}$	0.14 $^{+0.37}_{-0.11}$	8.79 $^{+9.34}_{-5.84}$	C
Gaia DR2 6045505569684851456	Gaia DR2 6045517286362149888	0.02 $^{+0.17}_{-0.20}$	0.82 $^{+0.66}_{-0.31}$	8.53 $^{+7.06}_{-4.70}$	C
Gaia DR2 6046055943965657856	Gaia DR2 6049110039371711232	0.49 $^{+0.20}_{-0.20}$	0.84 $^{+0.87}_{-0.43}$	7.44 $^{+1.69}_{-1.51}$	C
Gaia DR2 6050496459111584384	Gaia DR2 6051735162041951616	-0.51 $^{+0.19}_{-0.23}$	0.88 $^{+1.32}_{-0.34}$	7.78 $^{+3.02}_{-2.59}$	C
Gaia DR2 6053025507724358784	Gaia DR2 5861241504060387328	0.13 $^{+0.56}_{-0.79}$	0.31 $^{+0.12}_{-0.02}$	4.15 $^{+4.47}_{-2.88}$	C
Gaia DR2 6053025507724358784	Gaia DR2 5861249509876340096	-0.23 $^{+0.43}_{-0.37}$	0.54 $^{+0.69}_{-0.13}$	2.79 $^{+2.46}_{-1.40}$	C
Gaia DR2 6053028978057952256	Gaia DR2 5861209416444946816	0.67 $^{+0.57}_{-0.28}$	0.88 $^{+0.84}_{-0.48}$	9.14 $^{+4.85}_{-4.56}$	C
Gaia DR2 6053028978057952256	Gaia DR2 5861249509876340096	0.12 $^{+0.45}_{-0.58}$	0.83 $^{+0.57}_{-0.38}$	2.42 $^{+1.57}_{-0.99}$	C
Gaia DR2 6053693083047384576	Gaia DR2 6053774103316625664	0.73 $^{+0.62}_{-0.26}$	0.66 $^{+0.51}_{-0.10}$	6.91 $^{+3.45}_{-3.38}$	C
Gaia DR2 6054195353727048960	Gaia DR2 6054163296087784960	-1.53 $^{+0.38}_{-0.69}$	0.38 $^{+0.16}_{-0.11}$	4.33 $^{+1.32}_{-1.32}$	C
Gaia DR2 6054195353727048960	Gaia DR2 6058916136904260096	1.60 $^{+0.37}_{-0.28}$	0.87 $^{+1.08}_{-0.55}$	7.96 $^{+1.62}_{-1.54}$	F
Gaia DR2 6054752668651631872	Gaia DR2 6054691748830295168	-0.42 $^{+0.12}_{-0.19}$	0.72 $^{+0.05}_{-0.06}$	7.14 $^{+1.97}_{-1.97}$	C
Gaia DR2 6055724499479516544	Gaia DR2 6055724499479516800	0.00 $^{+0.16}_{-0.16}$	0.02 $^{+0.05}_{-0.01}$	2.20 $^{+2.38}_{-1.52}$	F
Gaia DR2 6057088443681190272	Gaia DR2 6057093112266125696	0.60 $^{+1.41}_{-1.93}$	0.67 $^{+2.39}_{-0.48}$	4.45 $^{+4.58}_{-2.87}$	C
Gaia DR2 6061991269115435136	Gaia DR2 6061962578725632640	-0.06 $^{+0.31}_{-0.25}$	0.54 $^{+0.06}_{-0.01}$	4.92 $^{+5.27}_{-3.40}$	C
Gaia DR2 6070080754075553792	Gaia DR2 6068230310365894400	-1.04 $^{+0.27}_{-0.43}$	0.86 $^{+0.43}_{-0.43}$	6.24 $^{+1.75}_{-1.71}$	C
Gaia DR2 6071348491003883136	Gaia DR2 6071087597518919040	-0.30 $^{+0.29}_{-0.51}$	0.95 $^{+0.32}_{-0.06}$	3.46 $^{+3.15}_{-2.17}$	C
Gaia DR2 6071348491003883136	Gaia DR2 6071307396762179200	-1.46 $^{+0.65}_{-1.89}$	0.60 $^{+0.42}_{-0.19}$	3.07 $^{+2.18}_{-1.95}$	C
Gaia DR2 6073430622416839296	Gaia DR2 6073227208454695424	0.30 $^{+0.18}_{-0.14}$	0.78 $^{+0.32}_{-0.19}$	6.38 $^{+2.03}_{-1.99}$	C
Gaia DR2 6074563978391541888	Gaia DR2 6074563978391541504	-0.24 $^{+0.74}_{-0.73}$	0.14 $^{+0.45}_{-0.11}$	1.55 $^{+1.47}_{-0.99}$	C
Gaia DR2 6074796250199371648	Gaia DR2 6074796245904371968	0.09 $^{+0.34}_{-0.45}$	0.19 $^{+0.49}_{-0.14}$	5.90 $^{+6.31}_{-4.00}$	C
Gaia DR2 6075374902576831616	Gaia DR2 6061305448711222400	1.38 $^{+0.01}_{-0.01}$	0.85 $^{+0.79}_{-0.58}$	8.83 $^{+0.16}_{-0.16}$	F

Table 6 continued

Table 6 (continued)

Star 1	Star 2	t_{ca} (Myr)	d_{ca} (pc)	v_{rel} (km s $^{-1}$)	Category
Gaia DR2 6075815841096386816	Gaia DR2 6075816592695096576	$-0.21^{+0.17}_{-0.21}$	$0.31^{+0.45}_{-0.19}$	$3.65^{+2.69}_{-2.04}$	C
Gaia DR2 607877306935807616	Gaia DR2 6078074169250372736	$-1.82^{+0.30}_{-0.39}$	$0.84^{+0.65}_{-0.43}$	$9.62^{+1.48}_{-1.47}$	C
Gaia DR2 6080080090775083392	Gaia DR2 6068961863556280832	$0.73^{+0.01}_{-0.02}$	$0.80^{+0.72}_{-0.36}$	$8.66^{+0.18}_{-0.18}$	F
Gaia DR2 6080080090775083392	Gaia DR2 6080072286810323968	$0.25^{+0.23}_{-0.18}$	$0.49^{+0.44}_{-0.10}$	$3.96^{+2.43}_{-1.78}$	C
Gaia DR2 6084425360726815360	Gaia DR2 6081530720270030208	$2.05^{+1.32}_{-0.61}$	$0.91^{+1.81}_{-0.60}$	$8.54^{+3.52}_{-3.47}$	C
Gaia DR2 6086467149517306368	Gaia DR2 6134516941522596352	$-0.07^{+0.20}_{-0.19}$	$0.81^{+0.34}_{-0.28}$	$4.27^{+0.81}_{-0.79}$	C
Gaia DR2 6088264477373916032	Gaia DR2 6088154010814701568	$0.65^{+0.52}_{-0.26}$	$0.84^{+0.30}_{-0.30}$	$7.90^{+3.43}_{-3.38}$	C
Gaia DR2 6090072894822497280	Gaia DR2 6090088769021601792	$1.26^{+1.51}_{-0.56}$	$0.76^{+0.97}_{-0.23}$	$8.01^{+5.16}_{-4.83}$	C
Gaia DR2 6106992866945163904	Gaia DR2 6107169755177631872	$0.56^{+1.04}_{-1.38}$	$0.92^{+2.39}_{-0.40}$	$5.65^{+5.68}_{-3.46}$	C
Gaia DR2 6108518340549366656	Gaia DR2 6108424740322313600	$0.39^{+1.29}_{-1.47}$	$0.84^{+2.35}_{-0.68}$	$2.79^{+2.42}_{-1.58}$	C
Gaia DR2 6124952431621117056	Gaia DR2 6124951400828926976	$-0.50^{+2.28}_{-1.45}$	$0.49^{+1.11}_{-0.27}$	$5.48^{+5.89}_{-3.79}$	C
Gaia DR2 6125358151409872256	Gaia DR2 6125358151409872512	$-0.23^{+0.12}_{-0.13}$	$0.21^{+0.17}_{-0.12}$	$7.57^{+1.31}_{-1.31}$	C
Gaia DR2 613034536147985024	Gaia DR2 6131956458118782208	$-2.28^{+0.53}_{-0.90}$	$0.93^{+0.89}_{-0.60}$	$8.16^{+2.35}_{-2.31}$	C
Gaia DR2 6203184676791371520	Gaia DR2 6203189762032648448	$-0.51^{+1.23}_{-1.08}$	$0.90^{+2.04}_{-0.61}$	$3.46^{+3.25}_{-2.05}$	C
Gaia DR2 6204835284262018688	Gaia DR2 6204835795359050752	$-0.58^{+0.39}_{-0.65}$	$0.48^{+0.93}_{-0.34}$	$3.06^{+2.34}_{-1.83}$	C
Gaia DR2 6237422850406493952	Gaia DR2 6240333803140170880	$-0.80^{+0.34}_{-0.61}$	$0.93^{+0.98}_{-0.56}$	$6.71^{+3.70}_{-3.27}$	C

NOTE—Star 1 are stars from the Sco-Cen sample and Star 2 are stars from the candidate and field star population. All identifiers are from *Gaia* DR2. The category column uses “C” and “F” to represent ScoCen-candidate encounters and ScoCen-field encounters.

Table 7. Simulated Potential Flyby Events from USCO Sample

Target Star	Flyby Star	$R\dot{V}_{sim}$ (km/s)	t_{ca} (Myr)	d_{ca} (pc)	d_{ca}/R_{HT}	d_{ca}/R_{HF}	Category	IR Excess?
HD 146285	2MASS J16172615-2450592	-3.76	-0.27 $^{+0.10}_{-0.11}$	0.30 $^{+0.18}_{-0.09}$	0.17 $^{+0.10}_{-0.05}$	0.34 $^{+0.20}_{-0.10}$	TF0.5	...
HD 145333	2MASS J16140211-2301021	-1.57	-0.65 $^{+0.28}_{-0.29}$	0.63 $^{+0.60}_{-0.38}$	0.44 $^{+0.41}_{-0.26}$	0.47 $^{+0.44}_{-0.28}$	TF0.5	...
HD 145333	2MASS J16140159-2258462	-3.08	-0.80 $^{+0.23}_{-0.26}$	0.44 $^{+0.42}_{-0.27}$	0.31 $^{+0.29}_{-0.19}$	0.46 $^{+0.44}_{-0.28}$	TF0.5	...
2MASS J16053815-2039469	[PGZ2001] J160517.9-202420	-7.30	-0.26 $^{+0.16}_{-0.28}$	0.33 $^{+0.27}_{-0.18}$	0.31 $^{+0.25}_{-0.17}$	0.40 $^{+0.33}_{-0.22}$	TF0.5	...
2MASS J1611742-1918285	K2-33	-1.23	-0.60 $^{+0.43}_{-0.49}$	0.36 $^{+0.22}_{-0.18}$	0.34 $^{+0.21}_{-0.18}$	0.43 $^{+0.27}_{-0.23}$	TF0.5	...
2MASS J16051687-1948374	HD 144273	-1.32	-0.58 $^{+0.50}_{-0.78}$	0.33 $^{+0.23}_{-0.12}$	0.29 $^{+0.20}_{-0.11}$	0.20 $^{+0.14}_{-0.08}$	TF0.5	...
UCAC4 355-076729	2MASS J16033829-1854076	-6.00	-0.24 $^{+0.15}_{-0.34}$	0.40 $^{+0.32}_{-0.20}$	0.41 $^{+0.33}_{-0.21}$	0.44 $^{+0.35}_{-0.23}$	TF0.5	...
HD 144925	[PGZ2001] J160900.7-190852	-2.38	-0.04 $^{+0.12}_{-0.12}$	0.35 $^{+0.05}_{-0.05}$	0.22 $^{+0.03}_{-0.03}$	0.36 $^{+0.06}_{-0.06}$	TF0.5	...
HD 147701	WSB 32	-5.92	-0.33 $^{+0.21}_{-0.23}$	0.72 $^{+0.73}_{-0.50}$	0.36 $^{+0.37}_{-0.25}$	0.68 $^{+0.68}_{-0.46}$	T0.5	...
HD 146285	REP 38A	-4.47	-1.18 $^{+0.13}_{-0.15}$	0.68 $^{+0.56}_{-0.33}$	0.39 $^{+0.32}_{-0.19}$	0.82 $^{+0.67}_{-0.40}$	T0.5	...
HD 146285	2MASS J16231145-2517357	-5.56	-0.90 $^{+0.12}_{-0.13}$	0.81 $^{+0.44}_{-0.25}$	0.46 $^{+0.25}_{-0.14}$	0.98 $^{+0.53}_{-0.31}$	T0.5	...
HD 146285	2MASS J16245302-2505561	-1.79	-1.20 $^{+0.14}_{-0.16}$	0.51 $^{+0.47}_{-0.28}$	0.29 $^{+0.27}_{-0.16}$	0.53 $^{+0.48}_{-0.29}$	T0.5	...
HD 146285	BKLT J162326-244822	-7.95	-1.00 $^{+0.11}_{-0.12}$	0.62 $^{+0.37}_{-0.27}$	0.35 $^{+0.21}_{-0.15}$	0.89 $^{+0.53}_{-0.38}$	T0.5	...
HD 145792A	2MASS J16121495-2440292	-8.27	-0.38 $^{+0.35}_{-0.40}$	0.79 $^{+0.42}_{-0.19}$	0.42 $^{+0.22}_{-0.10}$	1.19 $^{+0.64}_{-0.29}$	T0.5	...
HD 146706	EPIC 204206497	-4.71	-0.70 $^{+0.52}_{-0.77}$	0.76 $^{+0.44}_{-0.28}$	0.47 $^{+0.27}_{-0.13}$	0.87 $^{+0.50}_{-0.25}$	T0.5	...
HD 146706	2MASS J16171698-2259541	-7.34	-0.22 $^{+0.31}_{-0.34}$	0.75 $^{+0.41}_{-0.28}$	0.46 $^{+0.25}_{-0.17}$	1.08 $^{+0.59}_{-0.40}$	T0.5	...
HD 146367	2MASS J16151519-2252537	-5.27	-0.58 $^{+0.21}_{-0.39}$	0.50 $^{+0.38}_{-0.23}$	0.35 $^{+0.27}_{-0.16}$	0.87 $^{+0.67}_{-0.40}$	T0.5	...
2MASS J16261964-2137207	2MASS J16240942-2134075	-3.58	-1.10 $^{+0.51}_{-0.92}$	0.56 $^{+0.41}_{-0.27}$	0.59 $^{+0.43}_{-0.28}$	0.77 $^{+0.56}_{-0.36}$	T0.5	...
2MASS J16261964-2137207	2MASS J16220658-2127089	-2.24	-1.28 $^{+0.76}_{-1.09}$	1.37 $^{+0.86}_{-0.70}$	1.44 $^{+0.90}_{-0.73}$	1.87 $^{+1.17}_{-0.95}$	T0.5	...
EPIC 204637674	2MASS J16220658-2127089	-7.00	-0.58 $^{+0.45}_{-0.72}$	0.58 $^{+0.37}_{-0.28}$	0.49 $^{+0.31}_{-0.24}$	0.80 $^{+0.51}_{-0.38}$	T0.5	...
UCAC4 334-078461	EPIC 204190866	-4.53	-0.59 $^{+0.65}_{-0.90}$	0.50 $^{+0.27}_{-0.19}$	0.45 $^{+0.25}_{-0.17}$	0.64 $^{+0.35}_{-0.24}$	T0.5	...
HD 144587	2MASS J16084894-2400045	-3.14	-0.21 $^{+0.53}_{-0.62}$	0.70 $^{+0.36}_{-0.26}$	0.49 $^{+0.26}_{-0.18}$	0.98 $^{+0.51}_{-0.36}$	T0.5	T
HD 145333	2MASS J16181445-2319251	-8.99	-1.25 $^{+0.17}_{-0.19}$	0.61 $^{+0.48}_{-0.32}$	0.42 $^{+0.33}_{-0.22}$	0.96 $^{+0.76}_{-0.51}$	T0.5	...
HD 145333	2MASS J16183027-2245451	-7.45	-1.45 $^{+0.20}_{-0.22}$	0.64 $^{+0.60}_{-0.36}$	0.45 $^{+0.42}_{-0.25}$	1.02 $^{+0.95}_{-0.57}$	T0.5	...
HD 145468	2MASS J16114530-2254329	-6.17	-0.28 $^{+0.51}_{-0.59}$	0.59 $^{+0.82}_{-0.30}$	0.40 $^{+0.56}_{-0.20}$	1.05 $^{+1.47}_{-0.54}$	T0.5	...
2MASS J16042165-2130284	2MASS J16071199-2123472	-1.13	-0.82 $^{+0.37}_{-0.45}$	0.58 $^{+0.55}_{-0.45}$	0.45 $^{+0.42}_{-0.26}$	0.83 $^{+0.78}_{-0.48}$	T0.5	...
HD 146743	2MASS J16174810-2140322	-8.63	-0.77 $^{+0.85}_{-0.85}$	0.43 $^{+0.29}_{-0.14}$	0.31 $^{+0.21}_{-0.10}$	0.61 $^{+0.42}_{-0.20}$	T0.5	...
HD 145631	EPIC 205019241	-1.34	-0.49 $^{+0.34}_{-0.53}$	0.79 $^{+0.11}_{-0.31}$	0.49 $^{+0.07}_{-0.19}$	1.30 $^{+0.18}_{-0.51}$	T0.5	T

Table 7 continued

Table 7 (continued)

Target Star	Flyby Star	RV_{sim} (km/s)	t_{ca} (Myr)	d_{ca} (pc)	$d_{\text{ca}}/R_{\text{H,T}}$	$d_{\text{ca}}/R_{\text{H,F}}$	Category	IR Excess?
HD 145631	[PBB2002] USco J161052.4-193734	-1.47	$-0.50^{+0.36}_{-0.55}$	$0.75^{+0.34}_{-0.37}$	$0.46^{+0.21}_{-0.23}$	$0.91^{+0.42}_{-0.45}$	T0.5	T
HD 144925	2MASS J16033777-1845083	-8.11	$-1.43^{+0.27}_{-0.36}$	$0.67^{+0.52}_{-0.33}$	$0.43^{+0.33}_{-0.21}$	$0.75^{+0.58}_{-0.37}$	T0.5	...
HD 144925	2MASS J16044966-1850465	-4.33	$-0.81^{+0.21}_{-0.24}$	$0.55^{+0.50}_{-0.32}$	$0.36^{+0.32}_{-0.20}$	$0.91^{+0.82}_{-0.53}$	T0.5	...
HD 144925	2MASS J16040975-1833367	-1.27	$-1.10^{+0.17}_{-0.20}$	$0.59^{+0.37}_{-0.29}$	$0.38^{+0.24}_{-0.19}$	$0.80^{+0.51}_{-0.40}$	T0.5	...
UCAC2 2156782	Gaia DR2 6048725691338492800	-8.58	$-0.82^{+0.47}_{-0.49}$	$1.15^{+1.08}_{-0.66}$	$0.91^{+0.85}_{-0.52}$	$1.21^{+1.13}_{-0.70}$	F0.5	...
HD 147196	2MASS J16223000-2411228	-4.11	$-0.15^{+0.20}_{-0.17}$	$1.28^{+0.78}_{-0.43}$	$0.68^{+0.42}_{-0.23}$	$1.34^{+0.82}_{-0.45}$	F0.5	...
HD 146069	2MASS J16140159-2258462	-5.04	$-1.65^{+0.74}_{-1.63}$	$1.18^{+0.76}_{-0.63}$	$0.82^{+0.53}_{-0.44}$	$1.23^{+0.79}_{-0.66}$	F0.5	T
EPIC 204637674	2MASS J16220587-2121556	-6.77	$-0.15^{+0.35}_{-0.50}$	$0.92^{+0.25}_{-0.18}$	$0.77^{+0.21}_{-0.15}$	$0.96^{+0.26}_{-0.19}$	F0.5	...
HD 145333	2MASS J16223000-2411228	-4.53	$-1.76^{+0.23}_{-0.26}$	$1.37^{+0.70}_{-0.41}$	$0.95^{+0.49}_{-0.28}$	$1.44^{+0.73}_{-0.43}$	F0.5	...
BD-21 4301	2MASS J16140159-2258462	-3.10	$-1.16^{+0.38}_{-0.88}$	$1.33^{+0.34}_{-0.28}$	$1.01^{+0.26}_{-0.21}$	$1.40^{+0.36}_{-0.29}$	F0.5	...
2MASS J16085673-2033460	2MASS J16050978-1942146	-2.29	$-1.70^{+0.44}_{-0.61}$	$1.21^{+0.40}_{-0.38}$	$1.00^{+0.33}_{-0.31}$	$1.32^{+0.43}_{-0.42}$	F0.5	...
2MASS J16172297-2121119	2MASS J16132054-2229159	-1.39	$-2.00^{+0.48}_{-0.68}$	$1.26^{+0.80}_{-0.46}$	$1.30^{+0.82}_{-0.48}$	$1.38^{+0.87}_{-0.50}$	F0.5	...
ScoPMS 45	[T64] 6	-6.83	$-1.35^{+0.90}_{-0.90}$	$1.15^{+0.54}_{-0.43}$	$0.94^{+0.45}_{-0.36}$	$1.20^{+0.57}_{-0.46}$	F0.5	...

NOTE—The notations in this table are the same as in Table 4. RV_{sim} represents the RV value of the flyby star, which do not have RV measurement, that outputs the minimum d_{ca} .